

promising in this regard. More detailed studies are required to understand the origins of the behavior and to see if large MR values can be obtained at room temperature and low fields. What has become more exciting is the natural evolution to multilayered heterostructures, such as the spin valve or the spin tunnel junctions. The next few years should bring considerable excitement to this area of research.

## BIBLIOGRAPHY

1. J. Goodenough, *Prog. Solid State Chem.*, **5**: 145, 1972.
2. K. Chahara et al., *Appl. Phys. Lett.*, **63**: 1990, 1993.
3. R. Von Helmholt et al., *Phys. Rev. Lett.*, **71**: 2331, 1993.
4. S. Jin et al., *Science*, **264**: 413, 1994.
5. G. C. Xiaong et al., *Appl. Phys. Lett.*, **66**: 1427, 1995.
6. C. Kwon et al., *J. Magn. Mag. Matls.*, in press.
7. S. Kaplan et al., *Phys. Rev. Lett.*, **77**: 2081, 1996.
8. K. Ghosh et al., *Phys. Rev. B, Condens. Matter*, in press.
9. H. Y. Hwang et al., *Phys. Rev. Lett.*, **77**: 2041, 1996.
10. H. L. Ju et al., *Phys. Rev. B, Condens. Matter*, **51**: 6143, 1995.
11. A. Gupta et al., *Phys. Rev. B, Condens. Matter*, **54**: 15629, 1996.
12. Y. Lu et al., *Phys. Rev. B, Condens. Matter*, **54**: 8357, 1996.
13. J. Z. Sun et al., *Appl. Phys. Lett.*, **69**: 3266, 1996.
14. T. S. Ravi et al., *Phys. Rev. B, Condens. Matter*, **42**: 10141, 1990.
15. N. D. Mathur et al., *Nature*, in press.
16. M. Johnson and R. H. Silsbee, Interfacial charge-spin coupling: Injection and detection of spin magnetization in metals, *Phys. Rev. Lett.*, **55**: 1790, 1985.
17. M. Johnson, Bipolar spin switch, *Science*, **260**: 320, 1993.
18. M. Johnson, The all-metal spin transistor, *IEEE Spectrum*, **31**: 47, 1994.

R. RAMESH  
T. VENKATESAN  
University of Maryland

**MAGNETORESISTANCE, THERMAL.** See THERMAL  
MAGNETORESISTANCE.

## MAGNETOSTRICTIVE DEVICES

Magnetostrictive materials transduce or convert magnetic energy to mechanical energy and vice versa. As a magnetostrictive material is magnetized, it strains; that is, it exhibits a change in length per unit length. Conversely, if an external force produces a strain in a magnetostrictive material, the material's magnetic state will change. This bidirectional coupling between the magnetic and mechanical states of a magnetostrictive material provides a transduction capability that is used for both actuation and sensing devices. Magnetostriction is an inherent material property that will not degrade with time.

The history of magnetostriction began in the early 1840s when James Prescott Joule (1818–1889) positively identified the change in length of an iron sample as its magnetization changed. This effect, known as the Joule effect, is the most common magnetostrictive mechanism employed in magneto-

strictive actuators. A transverse change in dimensions accompanies the length change produced by the Joule effect. The reciprocal effect, in which applying a stress to the material causes a change in its magnetization, is known as the Villari effect (also referred to as the magnetostrictive effect and magnetoelastic effect). The Villari effect is commonly used in magnetostrictive sensors.

An additional magnetostrictive effect used in devices is the Wiedemann effect, a twisting that results from a helical magnetic field, often generated by passing a current through the magnetostrictive sample. The inverse Wiedemann effect, also known as the Matteucci effect, is used for magnetoelastic torque sensors (1,2).

The existence of both direct and reciprocal Joule and Wiedemann effects leads to two modes of operation for magnetostrictive transducers: (1) transferring magnetic energy to mechanical energy and (2) transferring mechanical energy to magnetic energy. The first mode is used in the design of actuators for generating motion and/or force and in the design of sensors for detecting magnetic field states. The second mode is used in the design of sensors for detecting motion and/or force; in the design of passive damping devices, which dissipate mechanical energy as magnetically and/or electrically induced thermal losses; and in the design of devices for inducing change in a material's magnetic state.

In many devices, conversion between electrical and magnetic energies facilitates device use. This is most often accomplished by sending a current through a wire conductor to generate a magnetic field or measuring current induced by a magnetic field in a wire conductor to sense the magnetic field strength. Hence, most magnetostrictive devices are in fact electromagnetoelastic transducers.

Some of the earliest uses of magnetostrictive materials during the first half of this century include telephone receivers, hydrophones, magnetostrictive oscillators, torque-meters, and scanning sonar. These applications were developed with nickel and other magnetostrictive materials that exhibit bulk saturation strains of up to 100  $\mu\text{L}/\text{L}$  (units of microlength per unit length). In fact, the first telephonic receiver, tested by Philipp Reis in 1861, was based on magnetostriction (3).

The discovery of "giant" magnetostrictive alloys (materials capable of over 1000  $\mu\text{L}/\text{L}$ ) in the 1970s renewed interest in magnetostrictive transducer technologies. Many uses for magnetostrictive actuators, sensors, and dampers have surfaced in the past two decades as more reliable and larger strain and force giant magnetostrictive materials (e.g., Terfenol-D manufactured by Etrema Products, Inc. and Metglas manufactured by Allied Corp.) have become commercially available (in the mid- to late 1980s). Current applications for magnetostrictive devices include ultrasonic cleaners, high-force linear motors, positioners for adaptive optics, active vibration or noise control systems, medical and industrial ultrasonics, pumps, and sonar. In addition, magnetostrictive linear motors, reaction mass actuators, and tuned vibration absorbers have been designed, whereas less obvious applications include high-cycle accelerated fatigue test stands, mine detection, hearing aids, razor blade sharpeners, and seismic sources. Ultrasonic magnetostrictive transducers have been developed for surgical tools, ultrasonic cleaners, and chemical and material processing.

The state of the art for commercially available magnetostrictive ultrasonic devices is a motor rated at 6 kW, with

development of a prototype 25 kW ultrasonic motor in progress (4). These motors are rated at resonance (20 kHz). Flex-tensional underwater sonar magnetostrictive devices have been driven to a source level of 212 dB (Ref. 1  $\mu$ Pa at 1 m) (5). Also, a recently designed high force test rig for use by the US Air Force in fatigue testing of jet engine turbine blades produces broadband forces from 200 Hz to 2000 Hz with peak to peak forces of 14 kN at 2 kHz (6).

## MAGNETOSTRICTIVE MATERIALS

All ferromagnetic materials exhibit magnetostriction; however, in many materials, its magnitude is too small to be of consequence. In the early 1970s, the search for a material that exhibited large magnetostriction at room temperature grew out of the discovery that the rare earth elements terbium and dysprosium exhibit magnetostriction (basal plane strains) on the order of 1% at cryogenic temperatures. From 1971 to 1972, Clark and Belson of the NSWC (Naval Surface Warfare Center) (7), and Koon, Schindler, and Carter of the NRL (Naval Research Laboratory) (8), independently and almost simultaneously discovered the extremely large room temperature magnetostriction of the rare earth-iron,  $RFe_2$ , compounds.

Partial substitution of other rare earths, such as dysprosium, for terbium in the Tb-Fe compound resulted in improvements in magnetic and mechanical properties. The stoichiometry of Tb-Dy-Fe that became known as the giant magnetostrictor Terfenol-D (terbium: Ter; iron: Fe; Naval Ordnance Laboratory: NOL; dysprosium: D) is given by  $Tb_xDy_{1-x}Fe_y$ , where  $x = 0.27$  to  $0.3$  and  $y = 1.92$  to  $2.0$ . Small changes in  $x$  and  $y$  can result in significant changes in the magnetic and magnetostrictive properties of the material. Decreasing  $y$  below 2.0 reduces the brittleness of the compound dramatically but reduces the strain capability. Increasing  $x$  above 0.27 does not significantly effect the strain capability, but it reduces the magnetocrystalline anisotropy, which effectively allows for increased magnetostriction at lower fields and more efficient energy transduction.

Nominal longitudinal strains for various materials are shown in Table 1. Note that nickel has a negative magnetostrictive constant, and its length shortens in the presence of a magnetic field, whereas other materials including Terfenol-D have a positive magnetostrictive constant. In the case of iron, the magnetostrictive constant changes from positive to negative, known as the Villari reversal, as the field is increased (9).

In 1978 Clark and co-workers (10) introduced a second new magnetostrictive material based on amorphous metal, produced by rapid cooling of magnetic alloys consisting of iron, nickel, and cobalt together with one or more of the following

elements: silicon, boron, and phosphorus. These alloys, known commercially as Metglass (metallic glass), have been processed to achieve very high coupling coefficients, on the order of 0.95, and are commonly produced in thin-ribbon geometries. Metglass is typically used for sensing applications and for converting mechanical or acoustical energy into electrical energy. The ease with which they can be magnetized and demagnetized and low core losses of these alloys constitute a distinct set of magnetic properties that have triggered high interest in research on metallic glasses (11).

Giant magnetostrictive materials are currently available in a variety of forms, including thin films, powder composites, and monolithic solid samples. Reviews of giant thin film magnetostrictive material are available (2,12,13). Giant magnetostrictive particle composites (GMPCs) and commercially available (Midé Technology Corp.) magnetostrictive elastomers are powdered magnetostrictive material (often Terfenol-D) solidified in a composite or rubber matrix (14). This form has the advantages that the nonelectrically conducting matrix material can be used reducing eddy current losses associated with ac operation, varied geometries are readily achieved, and the elastic properties, in particular ductility and machinability, can be greatly improved. Furthermore, devices using a driver element made with GMPCs as opposed monolithic material may avoid the need for prestress mechanisms and the bulky permanent magnets needed for biased ac operation. The major disadvantage with GMPCs is a reduction in output strain and strain rates related to the matrix-Terfenol-D composition ratio (14-17).

Some of the latest research on new magnetostrictive materials includes demonstration of a sputtered, amorphous thin film version of Terfenol-D and the doping of TbFeDy alloys with additional rare earths including holmium to minimize magnetic hysteresis losses (18). One of the most promising new research directions is work on magnetomemory materials, materials that combine the magnetostrictive behavior of ferroelectric materials with the high-strain attributes found in shape memory alloys. Currently, the FePdCo magnetomemory system exhibits magnetostriction several times that of the best giant magnetostrictive materials and is the focus of theoretical work by a number of researchers. Devices based on magnetomemory may provide significant advances in magnetostrictive sensor capabilities (19,20).

For this survey of magnetostrictive devices, applications using nickel and the monolithic forms of Terfenol-D will be emphasized, as these are the most common commercially available materials used in magnetostrictive transducer applications and are well suited for discussing common transducer design and operation issues.

## MAGNETOSTRICTIVE DEVICE TRANSDUCTION BASICS

Typical magnetostrictive transducers employ both electromagnetic energy conversion and magnetomechanical energy conversion. A wound wire solenoid is used for conversion between electric and magnetic energies, and a magnetostrictive material is used as the transducer driver to convert between magnetic and mechanical energies. For actuation, passing a current through the solenoid converts electrical energy into magnetic energy. Maxwell's equations can be used to show that the magnetic field seen by the magnetostrictive driver is

**Table 1. Nominal Strain of Magnetostrictive Materials**

Material	Magnetostriction ( $\mu$ L/L)
Iron	20
Nickel	-40
Alfenol 13	40
NiCo	186
Terfenol-D	2000

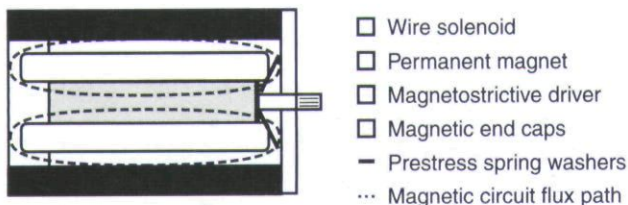


**Figure 1.** Components of basic magnetostrictive devices: magnetostrictive driver, magnetic end caps, permanent magnet, wound wire solenoid, magnetic circuit, and prestress mechanism.

proportional to the current in the solenoid. The magnetic energy generated by the solenoid simultaneously magnetizes and produces strain in the magnetostrictive core. This same device can also be used as a sensor. Application of a sufficient force to strain the transducer magnetostrictive driver will produce a change in the magnetization of the driver. In turn, this changing magnetic energy can be measured directly with a Hall probe or, as can be shown by using the Faraday–Lenz law, it can be converted to electrical energy in the form of an induced voltage in the solenoid and then measured. One of many common magnetostrictive device configurations is sketched in Fig. 1.

Figure 2(a) shows an output displacement versus applied magnetic field “butterfly” for a typical commercially available unbiased magnetostrictive actuator (Etrema Products Inc., Model AD-140j). For ac operation, either a dc current or a permanent magnet having a critical field strength of  $H_c$  is used to offset the initial actuator length, centering ac operation in the near-linear strain region. This is shown in Fig. 2(b) for a commercially available biased magnetostrictive actuator (Etrema Products, Inc., Model AA140j).

The efficiency with which a magnetostrictive material converts magnetic energy to mechanical and vice versa is often used as a key attribute to quantify the performance of a magnetostrictive device. It is noteworthy, however, that the design of a highly efficient magnetostrictive transducer also requires significant attention be paid to the efficiency of conversion between electrical energy and magnetic energy that actually goes into magnetization of the magnetostrictive driver. This requires careful design of the transducer magnetic circuit, including incorporation of a closed magnetic flux return path. This is a task that can be readily undertaken with modern finite element analysis tools. (See MAGNETIC CIRCUITS.)

Furthermore, proper matching of the system power supply to the input impedance of the transducer needs to be considered when optimizing overall system efficiency (just as a home stereo output impedance is matched to a standard 8 Ω loud speaker input impedance). The power supply rating in watts is equal to voltage times amperes and is given based on use with a specific load. Competing electrostrictive transducer technologies, based on piezoelectric and ferroelectric transduction, are capacitive devices that for generating moderate to high force output typically require power supplies capable of providing high voltages (on the order of 1000 V) at low currents (microamperes). Magnetostrictive transducers, on the other hand, are inductive devices that require power supplies capable of providing moderate voltages (less than 100 V to 200 V) at moderate currents (milliamperes up to several amperes) for similar force outputs. Depending on the power requirements and transducer design, the power supply for a magnetostrictive system could be similar to those used to drive common commercial electromagnetic devices, such as mechanical shakers and voice coil loudspeakers.

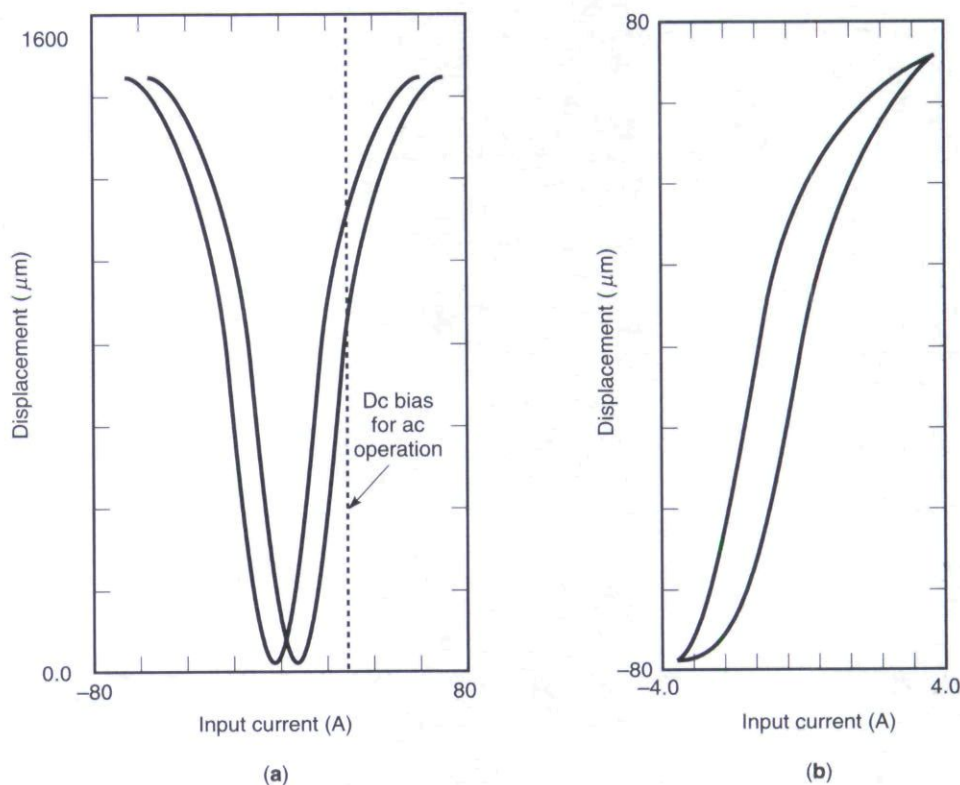


**Figure 2.** Commercially available magnetostrictive Terfenol-D actuator output: (a) unbiased Model AD-140j; (b) biased Model AA-140j. (Courtesy of ETREMA Products, Inc.)

The magnetostrictive effect itself is not frequency limited; however, in practice, ac losses (due to magnetic hysteresis and eddy currents) and device-specific mechanical and electrical resonances tend to restrict the output bandwidth capability to low ultrasonics (<100 kHz). Magnetostrictive devices do operate down to dc; a step input magnetic field will cause a step change in device length.

### THE MAGNETOELASTIC EFFECT

The magnetostrictive process relating the magnetic and mechanical material states can be described with the two coupled linear equations given in Eq. (1). These equations neglect temperature effects and have been reduced from a three-dimensional vector form to reflect only axial behaviors. These magnetostrictive equations of state are expressed in terms of mechanical parameters (strain  $\epsilon$ , stress  $\sigma$ , Young's modulus at constant applied magnetic field  $E_y^H$ ), magnetic parameters (applied magnetic field  $H$ , magnetic induction  $B$ , permeability at constant stress  $\mu^\sigma$ ), and two magnetomechanical coefficients (the axial strain coefficient  $d_{33} = d\epsilon/dH|_\sigma$  and  $d_{33}^* = dB/d\sigma|_H$ ),

$$\epsilon = \sigma/E_y^H + d_{33}H \quad (1a)$$

$$B = d_{33}^*\sigma + \mu^\sigma H \quad (1b)$$

These equations will be discussed in detail in a following section but for now should be considered as a basis for capturing the coupled mechanical and magnetic nature of magnetostriction. Equation (1a) indicates that the strain of a magnetostrictive element changes with stress and applied magnetic field. First, looking at the applied stress  $\sigma$ , when a stress is applied to a magnetostrictive sample, it will strain. If the field  $H$  is held constant and the stress varied, the sample will get shorter if the stress is compressive and longer if the stress is tensile. The magnitude of the effect is scaled by the inverse of the material's elastic modulus  $E_y^H$ . Next, an applied magnetic field  $H$  can also change the sample's length. If the stress is held constant, the effect of  $H$  in the strain is proportional to the applied field scaled by the piezomagnetic coefficient  $d_{33}$ . The elastic modulus and the piezomagnetic coefficients vary from one magnetostrictive material to the next and often vary with operating conditions. They need to be experimentally determined and are usually provided by the material manufacturer. Similarly, the magnetic induction  $B$  will also vary with stress and applied field, only scaled by the coefficients of Eq. (1b) as indicated.

Figure 3 shows a cartoon to help depict the strain and magnetic induction observed in magnetostrictive materials as they are magnetized and as described by these equations. In Fig. 3, the essence of a magnetostrictive device is lumped into discrete mechanical and magnetic attributes that are coupled in their effect on the magnetostrictive core strain and magnetic induction (21). As shown, the external stress is set to a constant compressive value ( $\sigma = \sigma_0$ ) provided by the mass resting on a stiff spring on top of the magnetostrictive core.

Looking first at the case of no applied field ( $H = 0$ ), the sample has an initial length ( $\epsilon = 0$ ), and no net axial magnetic induction ( $B = 0$ ), as depicted in Fig. 3(c). As the magnitude of the applied field  $H$  increases to its saturation limits,  $\pm H_s$ , the elliptical magnets rotate to align with the applied

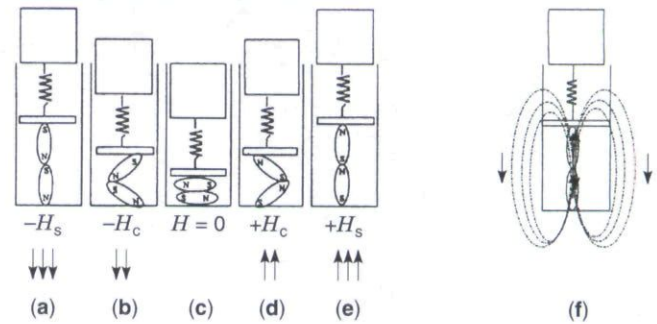


**Figure 3.** Cartoon of changing strain  $\epsilon$  and magnetic induction  $B$  in a magnetostrictive element subjected to a constant compressive stress  $\sigma_0$ . The applied magnetic field  $H$  increases from (a)  $-H_s$  through (c)  $H = 0$  to (e)  $H_s$ . Figure (f) indicates the magnetic flux lines associated with magnetization of the driver shown in (e).

field; the axial strain increases to  $\epsilon_s$  and magnetization of the element in the axial direction increases to  $+B_s$  [(Fig. 3(e)) or decreases to  $-B_s$  [(Fig. 3(a))]. At an applied field strength of  $H_s$ , the saturation magnitudes of strain and magnetic induction have been reached; that is, the strain and magnetization of the sample will not change with further increases in the applied field. Thus, both the magnetically induced strain and the magnetic induction magnitudes increase moving from the center figure outward as the magnitude of the applied field increases to its saturation values.

Alternatively, picture the applied field being set to a constant, like  $H_s$ , and then placing an increasing mass load or compressive force on the magnetostrictive element from the outermost figures to the center figure. Both the axial strain and axial magnetization magnitude in the element will decrease with increasingly negative (compressive) stress.

Figure 3(f) shows the flux lines associated with alignment of the magnetic domains in the magnetostrictive driver shown in Fig. 3(e). These lines are technically the superposition of the contributions caused by the magnetization of the magnetostrictive driver element and the applied field  $H_s$ . Flux lines for Fig. 3(a) would be similar in shape, but flux would be flowing in the opposite direction. Similarly, Figs. 3(b,d) would exhibit the same shapes in the appropriate direction but would be lower in magnitude. Figure 3(c) would not exhibit external flux lines, as the driver as shown is demagnetized. The flux field is used in sensors to measure the magnetization, strain, and/or force on the magnetostrictive driver by monitoring the flux either with a Hall effect probe or by detecting the voltage induced in a wire conductor perpendicular to the flux lines.

Even though this cartoon is not to be taken literally, it conveys the essence of the behaviors observed in magnetostrictive materials. For instance, the cartoon suggests that for ac applications, a dc magnetic bias can be applied to strain the material to half its saturation length and cycle between initial and saturated lengths. While this does convey the idea behind biasing, in practice the dc bias needed for ac operation,  $H_c$ , is based on operation centered in the steepest region of the curve shown in Fig. 2 where the strain-field slope is a maximum. This region, called the "burst" region, arises as a result of reorientation of magnetic moments (produced at the atomic level by electron spins) from an "easy" crystallographic

axis perpendicular to the applied field to one more closely aligned with the applied field. Easy axes correspond to orientations for the magnetic moment vectors that satisfy local crystallographic energy minimization states in the magnetostrictive material as the applied stress and magnetic field vary.

Furthermore, an initial compressive stress is often used to increase the alignment of magnetic moments along easy axes perpendicular to the applied field. Although a given sample cannot get any longer than its saturation length [Figs. 3a,e], under a prestress the sample's zero field length can decrease [get shorter than shown in Fig. 3(c)], thereby maximizing the net achievable strain.

## MAGNETOSTRICTIVE ACTUATORS

Numerous types of magnetostrictive transducers are distinguished by their configuration and use of the magnetostrictive driver. Common transducer classifications can be found in the literature (22,23). In most cases, the Joule effect in a magnetostrictive element is employed to produce a longitudinal vibration in rods or radial vibrations of tubes or rings. The most common design is the longitudinal vibrating Tonpitz in which a cylindrical or rectangular sample provides axial output (22). The tube-and-plate or tube-and-cone transducers use 1/4 wavelength magnetostrictive tubes to excite blocks tuned to transfer mechanical power to the surrounding medium efficiently. Other designs employ a number of magnetostrictive elements fitted end to end to form a ring or polygon (24). The simultaneous longitudinal excitation of the elements causes the ring's diameter to oscillate. The flextensional design (23) employs a longitudinal vibrating magnetostrictive element to excite an arched membrane, commonly an oval-shaped shell. Transducer designs have also been based on other magnetostrictive effects, such as the Wiedeman-effect twisting pendulum (2). Many variations in design on these transducers are available including some uses in noncontact activation, where, for instance in rotating environment, a nonrotating magnetic field source can be used to produce and/or sense shape changes in a rotating element.

Prior to the 1940s, the materials conventionally used for many transducer applications were the magnetostrictive elements nickel, cobalt, iron, and their alloys Permendur, Permalloy, and so on. In the 1940s and 1950s, the emergence of piezoelectric ceramics barium titanate and lead zirconate titanate (PZT) led to higher efficiency transducer designs. The twofold increase in coupling coefficient of PZT over that of nickel provided higher transducer acoustic efficiencies and larger output powers in a number of applications. With the development of giant magnetostrictive materials in the 1970s, even higher transducer efficiencies are now achievable. The superiority of Terfenol-D over piezoelectrics in high-power applications has been extensively demonstrated. Moffett, Powers, and Clark (25) present a theoretical comparison of the power handling capability of Terfenol-D and PZTs. A more recent paper by Moffett and Clay (26) address the superiority of Terfenol over PZT in a barrel-stave flextensional transducer in which the active motor was either Terfenol-D or PZT, with the rest of the device design otherwise unchanged. The Terfenol-D transducer had an FOM (figure of merit) of  $60 \text{ W/kg} \cdot \text{kHz} \cdot \text{Q}$ , about four times that of the PZT transducer, and an 8 dB higher source level throughout a

wider bandwidth. Akuta (27) reports a comparison of displacement versus output force relationships between PZT and Terfenol-D.

This should not be taken to imply that nickel-based actuators and sensors are outdated. Nickel still costs considerably less than giant magnetostrictive materials and shares the magnetostrictive attribute that (unlike their piezoelectric and ferroelectric counterparts) the magnetostrictive shape change capability will not degrade with use. Companies such as Blue Wave Ultrasonics offer commercial nickel-based ultrasonic cleaners with "the only lifetime guarantee in the industry."

## Performance Evaluation

Many techniques to characterize a transducer's performance are available. The technique selected usually depends on several factors, including the intended use of the transducer and allowable resources. Performance quantification in many cases boils down to analysis of the material properties under as-run conditions, that is, material properties of the active driver element based on measurements taken in the transducer under loads typical of a given application.

Magnetostrictive material properties are intrinsically related to the material magnetization, stress, and temperature distribution in the transducer. In fact, this relationship is strongly coupled so changes in operative parameters affect material properties and vice versa (28). Typical material properties considered when analyzing magnetostrictive transducers include Young's modulus, mechanical quality factor, magnetic permeability, saturation magnetization and magnetostriction, magnetomechanical or piezomagnetic coefficient, and magnetomechanical coupling factor. Measurements of a transducer performance provide magnetoelastic parameters that are characteristic of both the magnetostrictive driver and the transducer itself. For instance, the magnetomechanical coupling gauges the energy conversion between the elastic and magnetic sides of the device magnetostrictive material. However, in a transducer, the effectiveness of the energy conversion is highly dependent upon the magnetic circuit that routes the field applied by current through a solenoid into the driver. The magnetomechanical coupling then represents, when considered *in the transducer*, a property of both the driver and the specific transducer design. On the other hand, the saturation magnetization and magnetostriction are properties of the driver material itself, not the transducer. Further treatment on material property analysis can be found in Refs. 21,29-31.

To illustrate how these elastomagnetic properties relate to some important transducer performance indicators, we discuss six very distinct measures of transducer performance: (1) the strain-applied field ( $\epsilon-H$ ) characteristic curve, (2) transducer electrical impedance mobility loops, (3) transducer blocked force, (4) output energy and energy densities, (5) output power limitations, and (6) figures of merit.

**$\epsilon-H$  Characteristic Curve.** The idea of measuring quasi-static transducer displacement response for performance characterization has been explored extensively, mostly because of the simplicity of the procedure. The magnetic field intensity is, for a given input current, determined by knowledge of the solenoid characteristics, and the mechanical output is measured with displacement sensors such as the LVDT

(linear variable differential transformer) or accelerometers. Typical strain measurements at different mechanical preloads are shown in Fig. 4. A strain-applied field characteristic curve aids in choosing the optimum polarization field for achieving quasi-linear performance and for avoiding frequency doubling. Additionally, it provides information about some of the longitudinal elastomagnetic coefficients.

Returning to the coupled linear equations given in Eq. (1), which are known as the piezomagnetic constitutive equations, we see that, for fixed stress, the strain and applied magnetic field are related by the piezomagnetic coefficient  $d_{33}$ , with  $d_{33} = (\partial/\partial H)\epsilon|_{\sigma}$ , the slope of the  $\epsilon$ - $H$  characteristic curve. This is a very common measure of performance as a first look at a transducer's output capability. A value for  $d_{33}$  can be obtained by estimating the slope of a line drawn between the minimum and maximum strains for the rated output based on transducer data such as that shown in Fig. 2. Note that this may not be the same as placing a line on the tip and tail of the hysteresis loop shown in Fig. 2(b).

By forgoing the last 10% of achievable strain at the saturation and low field ends of the curve, much higher efficiency performance can be achieved. Trade-offs in quantifying a  $d_{33}$  based on measured data arise, whereby if additional displacement is required (assuming space and cost constraints allow for it), one may opt for using a longer sample in the steep region of the strain-field characteristic curve rather than driving a shorter sample to saturation. This would provide two device designs using drivers of the same magnetostrictive material with potentially quite different  $d_{33}$  coefficients.

This method for characterization of  $d_{33}$ , however, should be interpreted for use as measured (i.e., a dc measure of the transducer output). The differential values of  $d_{33}$  vary not only

with  $H$  and  $\sigma$  (see Figs. 2 and 4), but also with the magnetic bias, stress distribution in the material, and operating frequency (31,32). Hence the strain-field characteristic curve is of little use in assessing transducer dynamic operation, where the preceding factors play a significant role. In such cases, methods based on dynamic excitation of the transducer are preferred (31).

**Transducer Electrical Impedance Mobility Loops.** The total transducer electrical impedance, the electrical voltage measured per input current as a function of frequency, contains a plethora of information on transducer behavior. As discussed in detail by Hunt (3) and Rossi (33) among others, the electrical impedance is the sum of the blocked and the mobility impedances. The blocked impedance is the voltage per current associated with a transducer in which the output motion is restricted to zero, or "blocked." The mobility impedance is the difference in the total (measured) and blocked impedances and is a result of "mobility" or the force and velocity in the mechanical side of the vibrating transducer. (Although discussed here in the context of performance evaluation, understanding how to predict a transducer impedance function and having the ability to tailor its attributes for specific applications are also important with regard to power supply matching and optimization of total system performance.)

One use of impedance function information is to obtain fundamental resonant and antiresonant frequencies and the two associated elastic moduli for the magnetostrictive transducer driver. The resonant condition occurs when the magnitude of the mobility component of the measured impedance is its maximum and is represented by the diameter of the mobility impedance loop in the Nyquist representation (34). This resonant frequency  $f_r$  is associated with the open circuit (constant field) elastic modulus of the material  $E_Y^H$  so that  $f_r \propto \sqrt{E_Y^H}$ . Similarly, the maximum-diameter point of the electrical admittance loop ( $Y_e = 1/Z_e$ ) represents the antiresonant frequency  $f_a$  associated with the short circuit (constant induction) elastic modulus  $E_Y^B$ . This relationship is such that  $f_a \propto \sqrt{E_Y^B}$ .

The short circuit modulus  $E_Y^B$  represents the stiffest material condition, which occurs when all available magnetic energy has been transduced into elastic potential energy. When energy is transferred from the elastic to the magnetic side, the effective modulus decreases to the value  $E_Y^H$ . The two elastic moduli are related by the magnetomechanical coupling factor  $k$  ( $0 \leq k \leq 1$ ), as follows (35):

$$E_Y^H = (1 - k^2)E_Y^B \tag{2}$$

In a similar fashion, the intrinsic or uncoupled magnetic permeability  $\mu^\sigma$  of Eq. (1b) is reduced to a value corresponding to the constant strain permeability  $\mu^\epsilon$  because of the energy conversion from the magnetic to the elastic side. Clark (35) provides further detail and proves, by means of energy considerations, that both permeabilities are also related by  $k$

$$\mu^\epsilon = (1 - k^2)\mu^\sigma \tag{3}$$

By analogy to the cartoon in Fig. 3, holding the magnetic induction  $B$  constant while allowing  $\sigma$  and  $H$  to vary implies that the ellipses will not rotate from a given orientation. Hence the transducer will appear stiffer to an external force

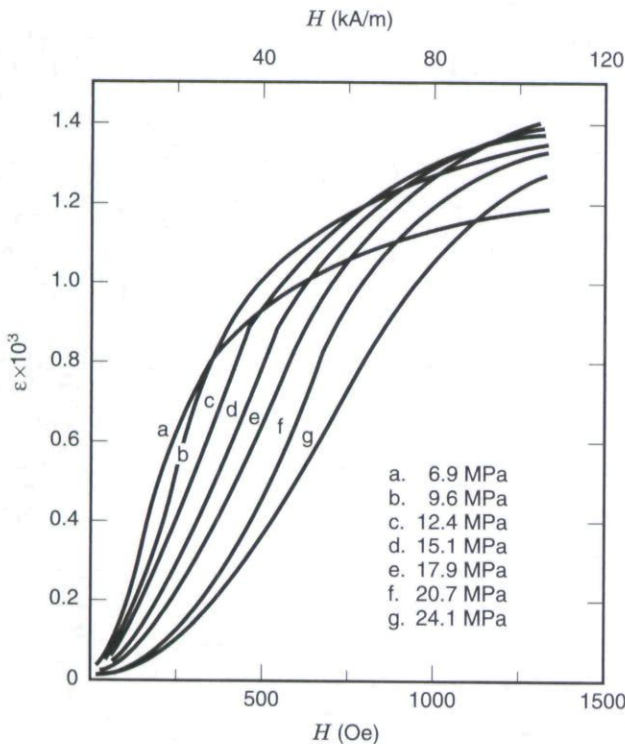


Figure 4. Strain-applied magnetic field relationship at 0.7 Hz, no magnetic bias, prestress: 6.9, 9.6, 12.4, 15.1, 17.9, 20.7, 24.1 MPa (32).

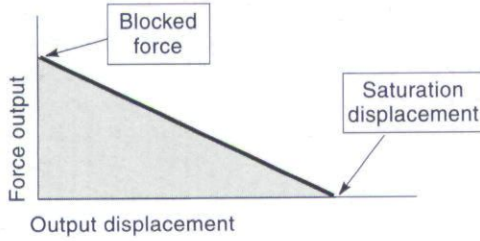


Figure 5. Cartoon of typical transducer blocked force–saturation displacement relationship.

than if  $H$  was held constant but  $B$  and  $\sigma$  were allowed to vary. Alternatively, holding strain  $\epsilon$  constant while varying  $H$  limits the potential change in  $B$ ; thus the material looks less permeable under operating conditions of constant strain than constant stress.

Ultimately, the electrical impedance provides information on how the energy is transferred between the magnetic and mechanical sides of the transducer. Knowledge of resonances  $f_r$  and  $f_a$  permits calculation of elastic moduli, magnetic permeabilities, and magnetomechanical coupling factor. Discussion on the latter will be continued in the “Figures of Merit” section.

**Blocked Force.** Figure 5 shows a sketch of a load line, a curve that represents the output force and displacement capabilities of a transducer. As the transducer tries to do work against an increasing load, its output displacement capability decreases. The system’s blocked force  $F_B$  is the load against which the transducer can no longer do work. At this load, the transducer displacement is reduced to zero, and the transducer is virtually “clamped” or “blocked.”

For a quasi-static loading case, a simplified transducer model can be developed using Newton’s Second Law which equates the force output of the transducer to an elongating elastic spring element,

$$F_T = k_m u_H \tag{4}$$

where the magnetostrictive driver material is assumed to have stiffness  $k_m$  and the transducer output displacement  $u_H$  is found as the magnetostriction [Eq. (1a)], times the driver length:  $u_H = \epsilon \times L$ . The effective stiffness of the driver, based on axial extension of a slender rod having a cross-sectional area  $A$ , length  $L$ , and short circuit elastic modulus  $E_Y^B$ , can be modeled as

$$k_m = \frac{E_Y^B A}{L} \tag{5}$$

Thus,  $F_T = E_Y^B A \epsilon$ . The transducer will elongate to its saturation length with a maximum force potential  $F_{Tmax} = E_Y^B A \epsilon_s$  under no external load. At the other extreme of the load line, an external load prevents strain of the magnetostrictive driver (hence the use of  $E_Y^B$  instead of  $E_Y^H$ ). Equating maximum external and internal force capabilities for no-strain and no-load, respectively, the blocked force rating for a transducer can be found as

$$F_B = E_Y^B A \epsilon_s \tag{6}$$

This force represents the maximum force that the material is capable of producing under quasistatic and lossless conditions, and it is a function of the rod geometry and the material properties  $E_Y^B$  and  $\epsilon_s$ . Based on published values of the short circuit elastic modulus  $E_Y^B = 50$  GPa and of the saturation magnetostriction  $\epsilon_s = 1600 \mu\text{L/L}$ , the blocked force rating for a device with a 24.5 mm diameter Terfenol-D driver is 38 kN.

**Output Energy and Energy Densities.** Let us assume a simple linear elastic load of stiffness  $k_L$  acting upon the Terfenol-D driver of stiffness  $k_m$ , as depicted in Fig. 6. Such a model represents, for instance, the actuator acting upon an acoustic load such as water and assumes no losses. The mechanical energy acting upon the load is

$$E_M = \frac{k_L u^2}{2} \tag{7}$$

where  $u$  is the displacement at the rod end.

One can separate the total displacement of the magnetostrictive driver into an active component and a passive component. The active component is the displacement of the driver free end  $u_H$  under no external load [Eq. (1a)]. The elastic or passive component is the response  $u_{el}$ , which opposes  $u_H$  as a result of the transducer doing work against an external load (possibly including work against a prestress mechanism). The total driver free end displacement is  $u = u_H - u_{el}$ .

The free end of the driver is subjected to a total force  $F$ , where the passive displacement is  $u_{el} = F/k_m$ , and the total end displacement is

$$u = u_H - \frac{F}{k_m} \tag{8}$$

For a linearly elastic external load, the force acting upon the driver end is  $F = k_L u$ . Substituting this expression for  $F$  into Eq. (8) yields

$$u = u_H - \frac{k_L u}{k_m} \tag{9}$$

or equivalently after defining  $t = k_L/k_m$

$$u = \frac{1}{1+t} u_H \tag{10}$$

Finally, substituting Eq. (10) into Eq. (7) and letting  $k_L = tk_m$  yields

$$E_M = \frac{t}{(1+t)^2} \left( \frac{k_m u_H^2}{2} \right) \tag{11}$$

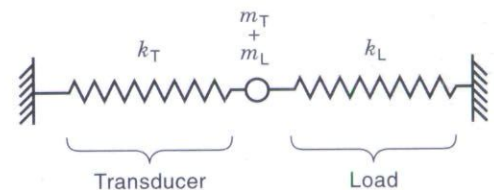
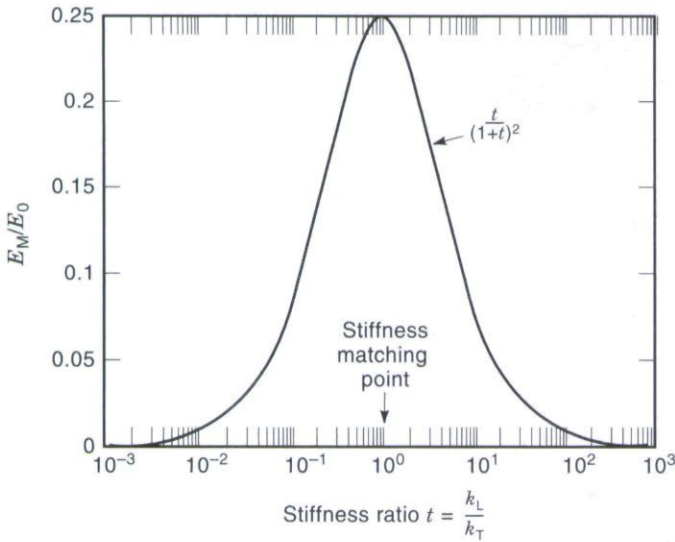


Figure 6. Schematic representation of an actuator of stiffness  $k_T$  loaded with an elastic load of spring constant  $k_L$ .



**Figure 7.** Normalized mechanical energy output is maximized for stiffness matching between the magnetostrictive driver and the combined transducer and external load stiffness characteristics.

This expression is plotted in Fig. 7 as a function of  $t$ , where it is readily apparent that the energy is maximum for  $t = 1$ . This situation indicates that stiffness matching is desired to achieve maximum output energy. It is also important to note that in some prestress mechanism designs, a spring or a set of washers is placed in series with the magnetostrictive driver. The spring stiffness has to be accounted for in calculations of stiffness matching. As noted previously, the driver stiffness is directly related to the elastic modulus  $E_y$ , which can be measured in different ways (28,30).

The output energy of a transducer is often scaled by the transducer volume, mass, and price. These energy “densities” facilitate the fair comparison between transducers. However, they do not give information on efficiency of energy conversion in the transducer. This issue is discussed further later.

**Projector Power Limitations.** As discussed in Refs. 36 and 37, the power output near resonance may be stress- or field-limited, depending on whether the mechanical quality factor  $Q$  is greater or smaller than the optimum value. This optimum  $Q$  hovers around unity for Terfenol-D (38). Hence, a low  $Q$  raises the maximum power limit of the transducer near resonance. In addition to the ability to handle more power output, a low  $Q$  means a broader operational bandwidth. This situation may or may not be desirable because at low  $Q$ , the transducer is less able to filter out unwanted modes of vibration that might lead to harmonic distortion. This highlights some of the compromises present in designing the transducer’s mechanical quality factor. Figure 8(a) depicts a typical radiated power limit- $Q$  curve indicating typical performance tradeoffs at frequencies near transducer resonance for a Terfenol-D transducer, and Fig. 8(b) presented an equivalent circuit representation of the transducer based on linear behavior.

**Figures of Merit.** The single most important transducer FOM is the magnetomechanical coupling factor  $k$ . This is particularly true in the low-signal linear regime, where  $k^2$  quan-

tifies the fraction of magnetic energy that can be converted to mechanical energy per cycle, and vice versa. Improvements in manufacturing techniques over the past decade have helped increase the magnetomechanical coupling factors reported in bulk samples of giant magnetostrictives like Terfenol-D. Today, values of  $k \approx 0.7$  are commonly reported for Terfenol-D ( $k \approx 0.3$  for nickel). Note that a transducer’s coupling factor will be lower than that of its magnetostrictive core due to magnetic, mechanical, and thermal losses inherent to other aspects of the device design and its components.

As discussed in detail in Ref. 35, rearrangement of the piezomagnetic equations (1a,b) leads to expressions for the magnetomechanical coupling on the basis that the energy transfer between elastic and magnetic sides in the Terfenol produces a change in the effective material elastic modulus and magnetic permeability. In a lossless scenario, the resonance and antiresonance frequencies of the electrical impedance function in Fig. 9(a-c) represent  $f_r$  and  $f_a$  as defined by the mobility impedance. In Fig. 9b, the prestress is constant at 1.0 ksi (kilopound per square inch) and in 9c the magnetic field is constant at 75 Oe. In the presence of losses,  $f_r$  and  $f_a$  shift slightly from the resonance and antiresonance points. Based on electroacoustic principles (3), it can be demonstrated that  $k$  is directly related to the system resonant and antiresonant fre-

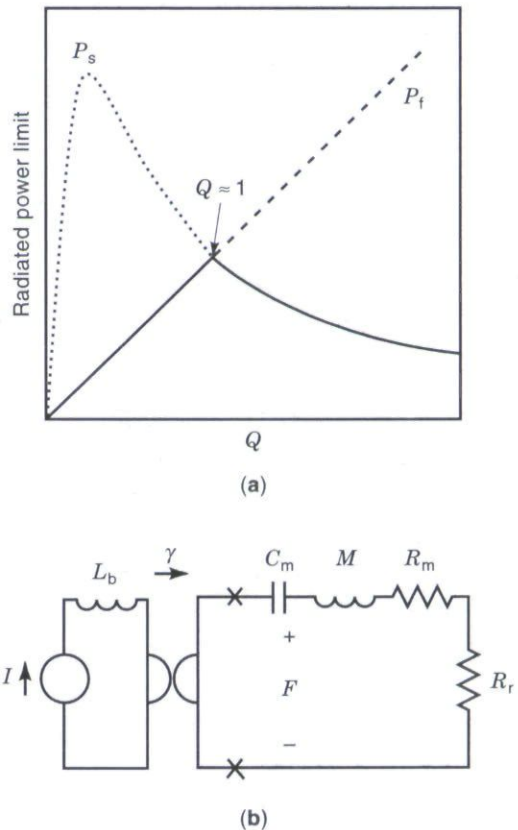


**Figure 8.** (a) Radiated power versus quality factor  $Q$  shown as the minimum of the stress limited output  $P_s$  and the field limited output  $P_f$ . (b) Van Dyke transducer equivalent circuit representation for the magnetostrictive device used to predict (a), where  $I$  = current,  $L_b$  = blocked inductance,  $\gamma$  = gyrator ratio,  $C_m$  = open circuit compliance,  $F$  = force,  $M$  = mass,  $R_m$  = mechanical resistance, and  $R_r$  = radiation resistance. Reprinted with permission from Ref. 36. Copyright © 1993 Acoustical Society of America.

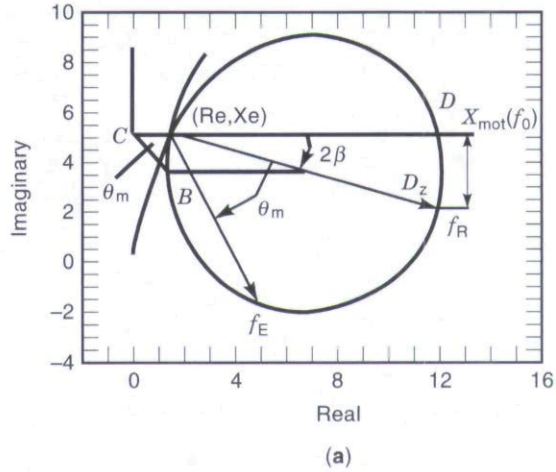
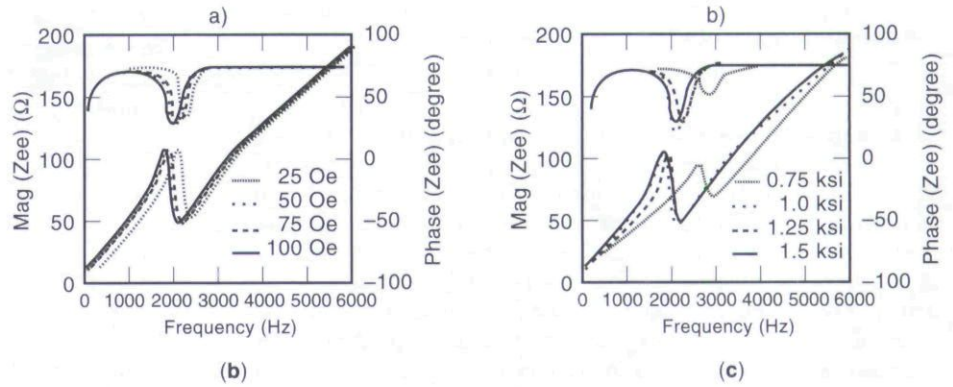


**Figure 9.** Measured Terfenol-D transducer electrical impedance functions: (a) Nyquist representation indicating diameter of mobility loop for use in determination of  $f_r$ ; (b) impedance for 1.0 ksi prestress at varied ac drive levels; and (c) impedance functions for 25 Oe drive level at varied initial prestress settings (39).



quencies,  $f_r$  and  $f_a$ . Assuming no losses,

$$k^2 = 1 - \left(\frac{f_r}{f_a}\right)^2 \tag{12}$$

The  $k$  dependence on ac field intensity and magnetic bias condition is clearly demonstrated in Refs. 28 and 39. In a lossy magnetic circuit, however, this relationship is somewhat different, although the essential aspects are preserved (28). The effect of losses can be minimized by carefully designing the magnetic path, and by using laminated material for the driver and all components of the magnetic circuit flux path by using either radial or longitudinal slots as appropriate. The penalty is typically increased complexity in manufacture and modeling.

An alternative formulation for  $k$  is derived from energy formulations, known as the three parameter method (35),

$$k^2 = \frac{d^2}{s^H \mu \sigma} \tag{13}$$

Transducers intended for underwater use are often rated according to the desired characteristics of these devices: high power  $P$ , low resonant frequency  $f_0$ , low mass  $M$  (or volume  $V$ ), and low quality factor  $Q$ . Hence, in the literature  $FOM = P/Qf_0V$  is commonly found. Claeysen et al. (40) present a comparison of several Terfenol-D and PZT devices with FOM

ranging between  $10 \text{ J/m}^3$  and  $655 \text{ J/m}^3$ , where a Terfenol-D flexensional has a remarkable  $655 \text{ J/m}^3$  figure of merit. A similar PZT device reached only  $15 \text{ J/m}^3$ ; the difference is caused exclusively by the much smaller strain output of the PZT (the acoustical power output is proportional to the strain squared).

**Types of Devices**

In order to illustrate the needs and issues of different transducer applications, we classify magnetostrictive transducers in three broad categories as follows:

1. High-power, low-frequency applications. These applications are typically associated with underwater acoustic generation and communications. The designs discussed here are the flexensional transducer, the piston-type transducer, and the ring-type transducer.
2. Motion generation. In this category, we include transducers designed to do work against external structural loads attached to them. The motion may be linear, such as in the inchworm or Kiesewetter motors, or rotational.
3. Ultrasonic applications. This category involves a fairly broad range of actuators, whose final use may actually vary from surgical applications to cleaning devices used in high-speed machining.

Despite the differences among the three categories, there is intrinsic commonality to all magnetostrictive devices based upon the magnetomechanical nature of the device. First of all, it is often desirable to achieve linearity in the performance. Because magnetostrictive materials respond nonlinearly to applied magnetic fields (hysteresis, quadratic response at low field, saturation at high fields), it is common practice to subject the material to mechanical and magnetic bias (known as bias conditions). A magnetic bias is supplied with permanent magnets, located in series or parallel with the drive motor, and/or with dc. The mechanical bias is applied by structural compression of the driver with either bolts or via the transducer structure itself, such as in flextensional transducers.

Second, maximum effectiveness is obtained at mechanical resonance, where dynamic strains of peak-to-peak amplitudes higher than the static saturation magnetostrain can be achieved. Dynamic strains are of primary importance in low-frequency, high-power transducers, namely those for sonar and underwater communications.

Among the other technological issues that affect the design and operation of magnetostrictive transducers are thermal effects, transducer directionality (determined by ratio between size and acoustic wavelength), resonant operation, and power source.

### Low-Frequency Sonar Applications

Research efforts searching for smaller sonar transducer systems capable of delivering increasingly higher acoustic power output have existed since the inception of sonar technology. Terfenol-D has proven attractive for underwater sound projection given its output strain, force, and impedance-matching characteristics. Not surprisingly, much of the research effort on magnetostrictive underwater devices has been performed by the US Navy, where Terfenol-D was originally developed.

The quest for more powerful sonar units forced researchers to increase either the size of the radiating surface or the vibration amplitude of the device. As a consequence, the former issue brought the re-emergence of a transducer principle first developed in the 1930s, the flextensional transducer. Magnetostrictive flextensional transducers offer high power at low frequencies. The power output of Terfenol-D flextionals is about 25 times larger than that of PZT flextionals because the dynamic strains are approximately five times larger and the power output is approximately proportional to the square of the strain. By comparison with the Tonpilz transducer, flextionals present the advantages of providing a larger radiating surface per volume, using less active material, and requiring lower voltages. Technological challenges inherent to flextionals are stress-induced fatigue, hydrostatic compensation, and prestressing for use in deep submersion. The Tonpilz-type transducer typically packs high power in a compact size. Moreover, because these transducers use an oversized piston for acoustic field generation, the diameter of the active element and magnetic circuit components can be increased without change in overall transducer diameter. A variation of the Tonpilz design is that with two end radiating surfaces, which have an impact on the radiated acoustic field's directivity pattern. Square-ring transducers are used in either omnidirectional or directional mode. They provide low-frequency acoustic emissions.

A discussion of actuator devices for sonar applications is presented next. The discussion addresses the three main types of devices: the flextensional, the ring-type, and the piston-type.

**Flextensional Actuators.** Flextensional transducers radiate acoustic energy by flexing a shell, usually oval-shaped, caused by the longitudinal extension and contraction of a cylindrical drive motor mounted in compression inside the shell. These transducers are capable of producing high power at fairly low frequencies. Their history dates back to 1929–1936, when the first flextensional device for use as a foghorn was first built and patented by Hayes at the NRL (41).

Several factors limited the effectiveness of the early flextensional devices. Hayes's original design lacked a preload mechanism, which limited the strain and force capability of the transducer and lead to fatigue-related failure. The parallel development in the late 1920s of the ring transducer, a relatively cheaper and more rugged device with similar electroacoustic efficiency, severely undermined the budget destined for research on flextionals. The flextensional concept was a high-power, high-efficiency transducer being used in the wrong field. It was not until the 1950s that flextionals started to be considered for underwater applications, leading to a 1966 patent by Toulis (42). This device was nearly identical to Hayes's, except for the explicit intention for underwater projection and the use of a piezoelectric stack for driving the device. Interestingly enough, the flextensional transducer is usually credited to Toulis (43).

Flextensional transducers are identified by classes. This is one aspect of flextionals that often leads to confusion among transducer designers. The confusion arises as to which geometry defines which class. To make matters worse, there are currently two different classification schemes and at least two proposed variations of those. With the exception of the Class I and IV, which are common to both schemes, the use of classification numbering must be accompanied by declaration of the scheme employed.

The following is a brief review of both classification schemes, as illustrated in Figs. 10(a,b). The reader is pointed to the references for further details.

In the classification scheme of Brigham and Royster (43,44), the radiating surfaces of Class I flextionals are formed by revolving an ellipse around its long axis. In other words, Class I flextionals have a football-shaped shell with the magnetostrictive motor mounted in compression inside, along the major axis. A variant of this design known as the University of Miami flextensional has flat surfaces as described in Ref. 43. The Class II flextensional is essentially a modified Class I in which, in order to accommodate more active material, the major axis is extended in both directions. The extra amount of active material allows more power handling without changing the fundamental resonance of the oval radiator. One strong limitation of the flextensional design is the lack of true broadband capability. To overcome this limitation, a Class III design has been proposed. The shell of the Class III flextensional consists of two Class I shells of slightly different sizes grated together. The two closely spaced resonances help to broaden the acoustic bandwidth beyond that of the Class I design. Unquestionably, the most common shell geometry is that of the Class IV flextensional. Typically, the shell is convex in shape, although there are variants, such as

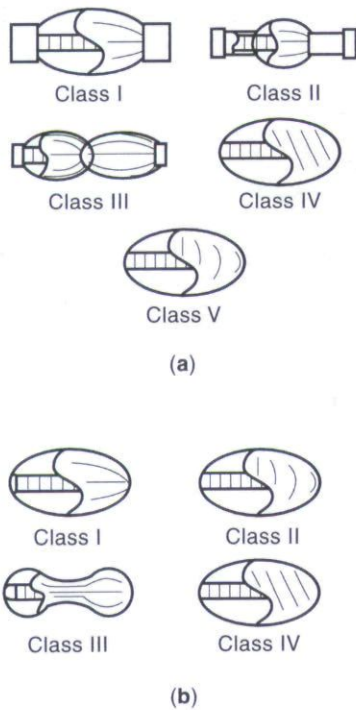


**Figure 10.** (a) Brigham and Royster's classification scheme for flextensional transducers. (b) Pagliarini and White's classification scheme for flextensional transducers.

the flat-oval shell or the concave shell of Merchant (classified type VII by Rynne) (45,46). Finally, the Class V consists of two shallow spherical caps attached to either side of a vibrating ring or disk (sometimes called clam shell). This design is credited to Abbott [however, this design had been described by Pallas in 1937 (23)], who in a 1959 patent (47), shows a ceramic-driven unit with either concave or convex spherical shells. Note that in the Brigham-Royster scheme, Classes I, IV, and V are basically distinguished by shape. On the other hand, Classes I, II, and III are differentiated by end use (i.e., Class II is a high-power version of Class I and Class III is a broadband version of Class I).

The Pagliarini-White scheme classifies flextensionals in four classes (I to IV), based exclusively on shell geometry (48-50). The Class I and Class II are similar to Brigham and Royster's Classes I and II. The Class III is known as the barrel-stave flextensional, and the Class IV is the typical oval-shaped shell. Jones (49) and Rynne (46) provide their own classification schemes by subtly modifying the previous schemes.

It is characteristic of flextensional transducers to have two types of radiating modes: a low-frequency flexing mode [or modes (51)] associated with the bending of the shell, and a higher-frequency breathing mode, in which the whole shell expands and contracts in unison. As the names implies, the desired mode of vibration is a flexural one. However, the breathing mode is acoustically more like a monopole; thus, it is usually of higher efficiency and improves the effective system magnetomechanical coupling factor. This higher mode has a strong effect on the parameters used to describe the flexural modes and, hence, it cannot be overlooked. Under hydrostatic pressure, the shell geometry determines whether the flexing mode occurs in phase or out of phase with respect

to the longitudinal vibration of the driver. The former case is characteristic of the Class IV flextensional, whereas the latter case is characteristic of Merchant's barrel-stave design.

In the Class IV design, the hydrostatic pressure acting on the shell tends to unload the magnetostrictive driver. This presents a technological challenge that defines the compromise between acoustic power and submersion depth. This problem has been addressed in different ways, including depth-compensation, mechanical filtering, and change of the shell geometry to concave instead of convex (Merchant).

In summary, flextensional devices designed for use with magnetostrictive drivers offer several advantages over other transducer materials such as PZTs, but successful demonstrations of their practicality for actuation are fairly recent. One such work reports a Terfenol-D-powered acoustic projector operated at a depth of 122 m (400 ft) driven to a source level of 212 dB (Ref. 1  $\mu$ Pa at 1 m) (5). Recent work (25,40) demonstrates that good magnetomechanical coupling and efficiency characteristics are possible in flextensional devices. Technological issues such as the magnetic circuit design, unloading of the magnetostrictive driver caused by submersion depths, the effects of cavitation at shallow depths, and stress-induced fatigue in the shell have been addressed effectively, even though trade-offs among these issues are inevitable (5).

**Piston-Type Actuators.** High dynamic strains are instrumental in achieving high acoustic power radiation. As with many other transducer designs, the availability of giant magnetostrictive materials such as Terfenol makes it possible to design more powerful underwater piston transducers with little or no bulk penalty. It has been suggested (40) that because of the need for much less active material, the cost of a Terfenol-driven piston transducer would be lower than, for instance, that of an equivalently rated piezoelectric flextensional transducer. The simpler design and the lack of bending parts likely to suffer fatigue-induced failure also indicate some of the advantages of piston-type designs over conventional flextensional transducers.

The Tonpiliz transducer (Tonpiliz is German for "sound mushroom") is quite simple in principle, as illustrated in Fig. 11. The magnetostrictive rod is surrounded by a drive solenoid, which provides the magnetic field excitation. The magnetostrictive element actuates upon an inertial mass ("tail"

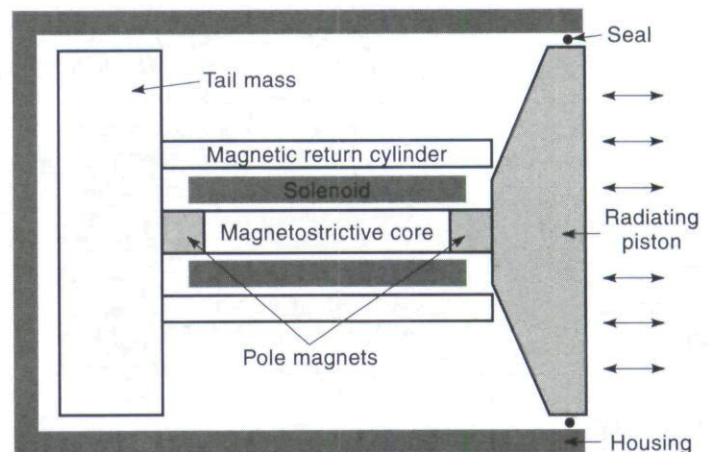


**Figure 11.** Typical Tonpiliz magnetostrictive transducer.

mass) and has a front radiating surface which generates the desired sound waves. The magnetic path is completed by magnetic couplers and a magnetic return path cylinder. In fact, the magnetic circuit can have many possible configurations. For instance, some designs use cylindrical permanent magnets and ferromagnetic end pieces known as a "barrel magnet" configuration instead of the "stacked magnet" configuration shown in Fig. 11. Each configuration has a specific set of merits, which means that the optimum magnetic circuit configuration should be identified based upon the particular application requirements (52). As a rule of thumb, rods shorter than 20 cm and with diameters under 2.5 cm have increased magnetic coupling, in the order of 5%, in the barrel magnet configuration over what can be achieved using a stacked magnet configuration (reference: T. T. Hansen of Extrema Products, Inc., personal communications). However, when longer and thicker rods are used, significant phenomena such as saturation and end effects are likely to occur in the barrel magnet configuration. The stacked magnet configuration does have the potential for significantly increasing the systems' resonant frequency due to stiff pole magnets located in series with the magnetostrictive element. Typical permanent magnet materials currently in use are Alnico V, samarium-cobalt, and neodymium-iron-boron, while the magnetic return materials currently used are laminated steel and ferrites.

Recently, researchers have been able to develop innovative magnetostrictive Tonpizl radiators capable of excellent source level outputs and very high FOMs. Steel describes (53) a Tonpizl transducer in which six hexagonal cylinders of Terfenol-D are arrayed forming a tube inside which there is a prestress rod. The transducer itself is mounted on its central node in such a way that the magnetostrictive tube and the head mass form a so-called balanced piston design. The vibration of head and tail masses is almost symmetrical (with the same velocity but in opposite directions). The advantage of this design is that the Terfenol-D tube is isolated from hydrostatic pressure and freed of undesirable shifts in resonant frequency as a result of changing preloads. However, balanced piston operation occurs only near resonance, so the device is a narrow bandwidth transducer.

Conversely, a novel hybrid magnetostrictive/piezoelectric transducer designed at the NUWC (Naval Underwater Warfare Center) (54) is capable of broadband operation by virtue of its double resonance configuration. The transducer consists of a series arrangement of a tail mass, an active driver, a center mass, a second active driver, and a head mass. Because the velocities of the piezoelectric and magnetostrictive drivers are  $90^\circ$  out of phase with each other, self-tuning similar to that in the balanced piston design is obtained. In addition, the improved coupling coefficient of this device translates into better acoustic response at even lower frequencies than in conventional Tonpizl transducers of similar size and weight.

Meeks and Timme (55) present a Tonpizl vibrator consisting of three Terfenol rods spaced  $120^\circ$  apart, head and tail masses, and a center rod for mechanical and magnetic biasing. The transducer was not as powerful as more recent units, but it was useful for demonstration of the potential of Terfenol-D for this type of application.

Claeyssen and Boucher (56) developed a set of magnetostrictive transducers capable of very high acoustic power output. An initial design, called the Quadripode, uses four rods

to vibrate the radiating piston at an in-water resonant frequency of 1200 Hz. A follow-up design, named Quadripode II, has better effective coupling and broader operational bandwidth, thanks to modifications in the head mass and prestress rod. Both transducers feature a forced cooling device. A transducer based on three rods instead of four, called Tripode, was also developed. It better uses the giant magnetostriction effect to yield twice the power output of the four-rod transducers (3.8 kW versus 1.6 kW), packed in less than half the volume ( $22 \text{ dm}^3$  versus  $51 \text{ dm}^3$ ). Hydrostatic compensation permits deep submersion up to 300 m. The source level of the Tripode at resonance (1.2 kHz) is 209 dB (Ref.  $1 \mu\text{Pa}$  at 1 m), and the FOM is  $24 \text{ J/m}^3$  (40). Another interesting design is the double-ended vibrator; a radiating piston replaces the tail mass so that the transducer is symmetric around its midpoint. This transducer competes favorably against the flex-tensional in the 300 Hz range because of its simpler, cheaper design, the lack of fatigue-related problems, and the lower voltages required for operation. More details on this device can be found in Refs. 40 and 56.

**Ring Actuators.** In a general sense, ring transducers employ the radial vibrations of tubes or plates. This concept was first developed during the late 1920s (23). The interest in ring transducers during those early days was based on the ruggedness and lower cost compared to other available transducer technologies. One example of those early magnetostrictive devices is the radially vibrating cylinder patented by Hayes in 1935 (57).

The ring transducer concept was extensively researched, not only with magnetostrictive materials as the active driver but also with piezoelectric ceramics (58,59). Today, the better coupling factor and lower elastic modulus of the rare earth iron alloys gives these materials an edge over conventional piezoelectrics.

For instance, the square ring transducer in Ref. 60 is a device capable of providing either omni- or directional sound propagation at low frequencies. Four Terfenol rods are arranged forming a square; the radiating surface consists of four curved pistons attached to each corner of the square, as shown in Fig. 12. A similar principle was utilized in the octagonal ring transducer discussed in Ref. 61.

One interesting feature of the square-ring transducer is its ability to generate either dipole or omnidirectional sound ra-

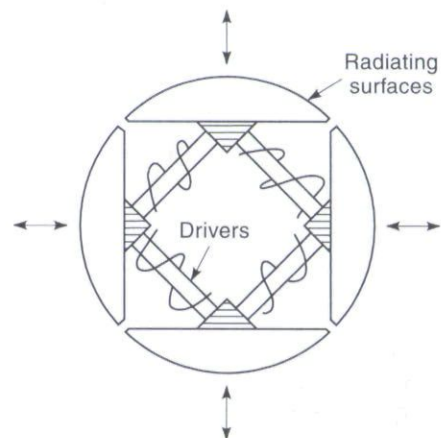


Figure 12. Schematic representation of a square-ring transducer.

diation. The dipole mode is accomplished by switching the magnetic bias on two of the rods and maintaining a constant direction on the ac magnetic field on all four rods. This feature translates into a transducer having two effective resonant frequencies and  $Q$  values, one for each mode of operation.

**Motion/Force Generation Devices**

There is growing interest in the use of magnetostrictive devices as a source for motion and/or structural forces. A variety of magnetostrictive motors have been designed, with the objective of providing accurate actuation at a given force rating over a range of operating frequencies. Conventional electromagnetic and hydraulic devices are commonly used in combination with gear boxes for motion conversion, and as a result are prone to mechanical play and bulkiness. Magnetostrictive motors produce outputs comparable to many conventional systems without the need for a gearbox interface, thereby avoiding many of the added system design issues (mass, volume, wear, play, backlash, etc.).

In this section we classify magnetostrictive motors as linear and rotational, depending on the type of motion provided by the device.

**Linear Motors.** The simplest type of linear motion device, a piston actuator, was presented in Fig. 1. Piston devices output mechanical strains and forces over bandwidths from dc to over 5 kHz. Piston actuators have been employed in a variety of applications, ranging from linear positioners and control of valves to achieving active vibration control in structures in single-ended configurations (62–65) and as active struts in double-ended configurations (66). The stroke of these devices is limited to the strain of the magnetostrictive driver element. The stroke can be increased by going to a longer device or using any of a variety of simple motion amplification devices, with the drawback of introducing play.

Magnetostrictive motors capable of displacement strokes greater than the core saturation strain include the elastic wave motor (EWM), or Kiesewetter motor (67). The EWM consists of a cylindrical Terfenol-D rod moving in inchworm-like fashion inside a stator tube. The magnetostrictive core is snugly placed inside the stator tube; the stator is in turn surrounded by several short coils located along its length. As the first coil is energized, the magnetostrictive element lengthens locally, while its diameter decreases by virtue of the volume invariance of the magnetostrictive effect. When the field is removed, the rod clamps itself again inside the tube. By energizing the coils sequentially along the length of the stator, it is possible to induce a displacement  $d_s$  per cycling of the coils as indicated in Fig. 13. The length of the step  $d_s$  can be adjusted by varying the magnetic field intensity generated by the coils. The speed of the motor is regulated by the speed at which the coils are energized and by the shielding effects of eddy currents. Normally the coils are excited with a single traveling pulse, but increased speed can be achieved by multiple-pulse excitation. Reversal of the direction of motion is achieved by reversing either the bias polarization or the direction of the traveling pulse. The device load handling rating is constrained by either the interference forces generated between the core and the stator tube or the blocked force capability associated with core elongation. A

prototype designed for use in the paper industry develops 1000 N of force, 200 mm of stroke, and 20 mm/s speeds (68). Other areas of application for this device are valve control and precision positioners. The EWM has also been utilized for active control of the profile of aircraft wings. The proof-of-concept device in Ref. 69 facilitates fuel savings in aircrafts of 3–6%, by changing the profile of the “smart trailing edge” at speeds of 0.4 mm/s and strokes of 25.4 mm.

A variant of the inchworm principle uses fixed-position and translating transducer elements to simultaneously clamp and unclamp adjacent sections of a load shaft. When the translating clamps are engaged, pusher transducers are actuated to move the translating clamps from their resting position. When the fixed position clamps are engaged, the pusher elements return the (now unclamped) translating elements to their resting position. The fixed position clamps maintain the load shaft position during the return portion of the translating clamps’ motion cycle. By sequential clamping and unclamping, bidirectional linear motion of the load shaft is in-

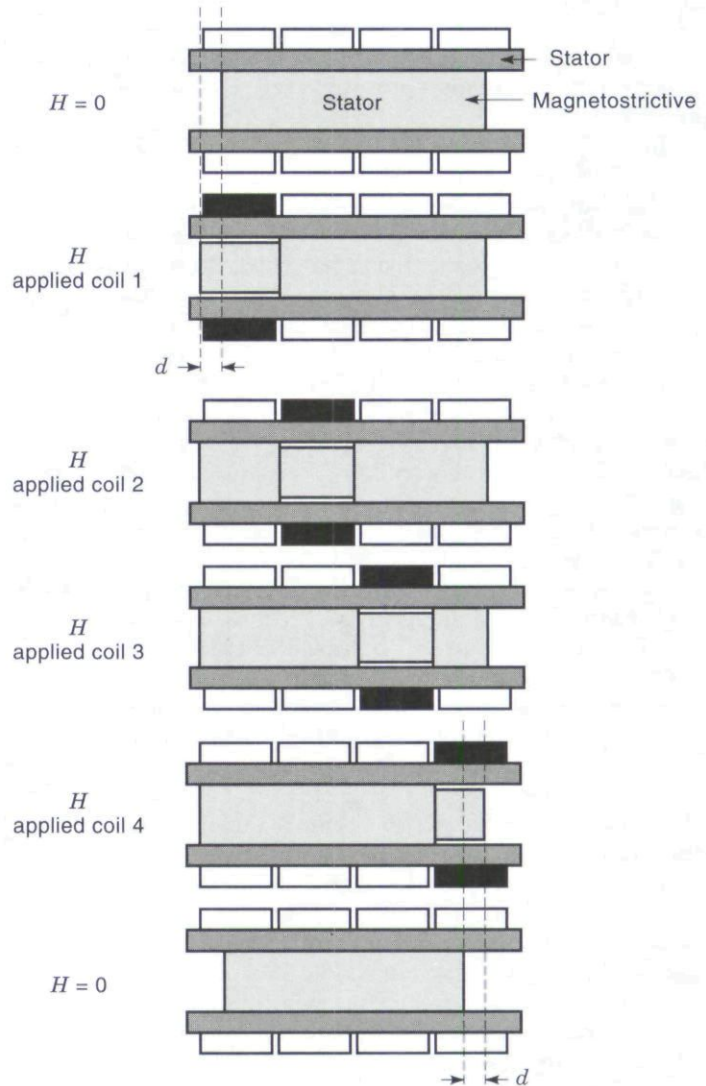


**Figure 13.** Principle of operation of the Kiesewetter inchworm motor. Energized solenoids are marked in black; passive solenoids are white.

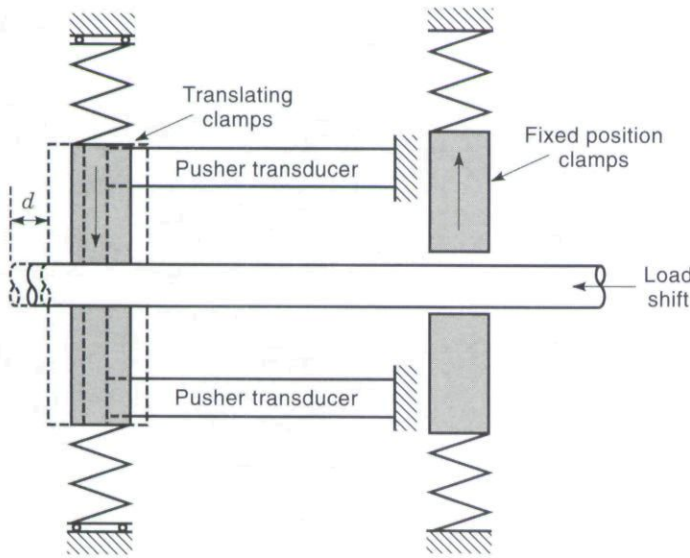


**Figure 14.** Principle of operation of the hybrid piezoelectric/magnetostrictive inchworm actuator.

duced as illustrated in Fig. 14. The device load handling rating is constrained by either the clamping forces generated between the load shaft and clamping transducer elements or by the blocked force capability associated with the pusher transducers.

Some researchers have demonstrated hybrid devices, in which both piezoelectric and magnetostrictive devices are employed. In Fig. 14 the clamping is done with piezoelectric stacks while translation is provided by Terfenol-D devices. A prototype motor of this kind is presented in Ref. 70. Designs employing an inchworm design using magnetostrictive clamps and piezoelectric pusher elements are also being studied (71). The attraction for design of hybrid devices arises when the motor is driven at its electrical resonance, characterized by the inductive and capacitive nature of the magnetostrictive and piezoelectric materials. The 180° phase lag between the piezoelectric stacks, and the 90° phase lag between the inductor current and the capacitor voltage, provide natural timing for the clamping, unclamping, and linear motion actions. In addition, the amplifier design is greatly simplified because of the significant reduction of the reactive power load (transducer impedance is almost purely resistive). The Fig. 14 prototype achieves a stall load of 115 N and no-load speeds of 25.4 mm/s. A similar idea (72) uses a magnetostrictive bar as a load shaft, allowing a very compact design. When used in conjunction with a dedicated switching power drive, the predicted speed of the motor is 7.8 mm/s, at a frequency of 650 Hz and force of 130 N. Other examples of linear magnetostrictive motors are the push-pull actuator by Kvarnsjo and Engdahl (73), the oscillating level actuator by Cedell et al. (15), and the broadband shaker by Hall (21).

**Rotational Motors.** The magnetostrictive principle has been lately employed in rotational motors as well. Several areas such as the aerospace and the automotive industries benefit from the higher controllability of the "smart material" motors compared to conventional hydraulic or electromagnetic devices. In particular, there is also a niche for high torque, low speed motors, in which the inchworm technique is particu-

larly suitable. A device having these characteristics, capable of a maximum torque of 3 N·m and speed of 3°/s, is presented by Akuta in Ref. 74. Another working prototype of the inchworm type is that presented by Vranish et al. (75), a quite sophisticated design capable of very high torque of 12 N·m at speeds of 0.5 rpm and precision microsteps of 800 microradians. Despite the great positioning accuracy and high holding torques, to date the inchworm-type devices sometimes lack in efficiency, which can represent a severe limitation in some applications. To overcome this, a resonant rotational motor based on a multimode stator has been proposed by Claeysen et al. (76). Two linear Terfenol-D actuators are used to induce elliptic vibrations on a circular ring (stator), which in turn transmits rotational motion to two rotors pressed against the ring. The prototype did not achieve the expected deficiencies, but at 2 N·m of torque and speeds of 100°/s, the potential of this idea has been clearly demonstrated. The vibrations of the stator are illustrated in Fig. 15.

A proof-of-concept hybrid magnetostrictive/piezoelectric rotational motor is illustrated in Fig. 16, following the concept presented in Ref. 77. A piezoelectric stack clamps a piece of friction material onto the rotating disk, while two magnetostrictive rods move the clamp tangentially to the disk to achieve rotational motion. The direction of induced motion is bi-directional, determined by the direction of excitation of the oppositely connected driving solenoids. Once again, the inductive and capacitive nature of the transducer's electrical impedance is used to minimize the reactive power requirement on the power amplifiers, and the timing is naturally determined by the time lag between inductors and capacitors. Thus operation near electrical resonance is ultimately desired. The prototype shown in Ref. 77 achieves near 4 rpm at excitation frequencies between 650 Hz and 750 Hz and voltages of between 30 V and 40 V.

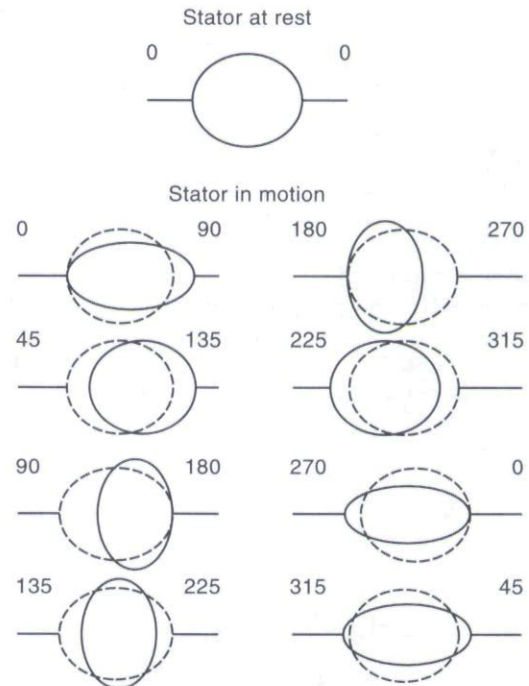


**Figure 15.** Modes of vibration of the rotational motor of Claeysen et al. (76).

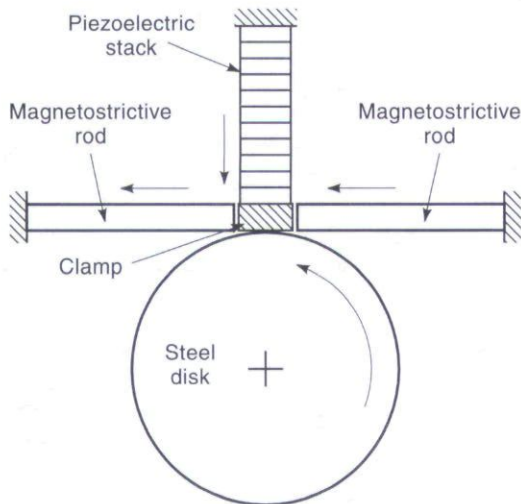


**Figure 16.** Hybrid piezoelectric/magnetostrictive rotational motor [after (77)].

Some of the rotational motors presented in this section lend themselves very well to ultrasonic frequencies. These devices, along with other types of ultrasonic transducers, are discussed in the next section.

**Ultrasonic Devices**

Ultrasonics is the science of acoustic waves with frequency above the human audible range, nominally above about 20 kHz. This definition is somewhat arbitrary, since most sound propagation phenomena behave the same at sonic and ultrasonic frequencies. However, the distinct features of ultrasonic devices merit a separate study from other types of transducers. For instance, one major problem in the generation of airborne ultrasound is the difficulty associated with coupling the energy generated by the electroacoustic device into the medium due to the large impedance ratio mismatches between the transducer and the medium (on the order of  $10^{-5}$ ). At very high frequencies in the megahertz range, the ultrasonic energy can be concentrated by shaping a thin film transducer into a bowl shape. The center of curvature represents the energy focus. An alternative way, usually employed at frequencies in the tens of kHz range, is by using a half-wavelength metal horn (the length of the horn is one-half the wavelength of elastic waves at the transducer's resonant frequency). The tapered shape of the horn produces an increase in the displacement, velocity, and pressure amplitudes, as illustrated in Fig. 17 (78). Note each profile has its own modal characteristics, thus the right shape must be carefully chosen for the application in hand.

Traditionally, the most common magnetostrictive materials used for ultrasonic applications were pure nickel and iron-cobalt alloys, such as Permendur (49% iron, 49% cobalt, 2% vanadium). The magnetostrictive material is shaped so that good closure of the magnetic flux is achieved, and several laminas of the material are stacked together to minimize eddy current losses. The power losses due to eddy currents are proportional to the square of the operating frequency, so at ultrasonic regimes their significance is high. The material is as usual driven with solenoids. These transducers are normally operated at the half-wave fundamental frequency, which

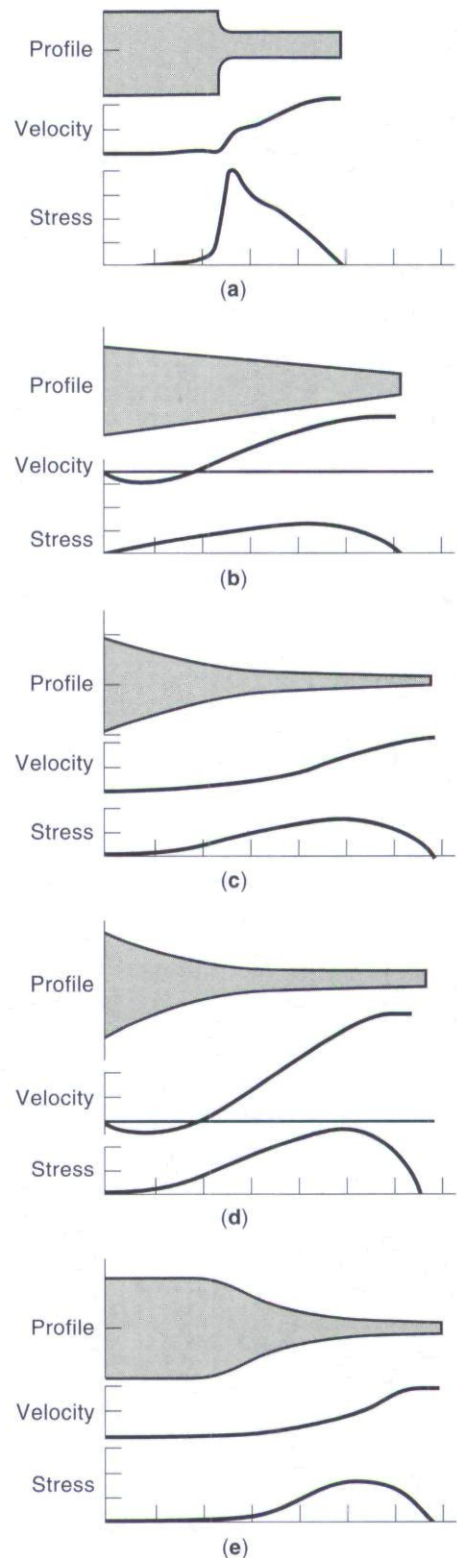


**Figure 17.** Geometry, velocity, and stress profiles of horns for amplifying the displacement output of ultrasonic transducers. (a) Stepped, (b) conical, (c) exponential, (d) catenoidal, (e) Fourier. (78) Reproduced with permission, copyright © John Wiley & Sons.

means there is a node in the center plane of the magnetostrictive element. This plane, where no motion is produced, constitutes a good mounting point for the transducer. Alternatively, if concentration of acoustic energy is sought through the use of a horn, the mounting point can be moved to the horn's node. This situation is illustrated in Fig. 18 (79).

Devices similar to that of Fig. 18, with or without the coupling horn, are being used in diverse applications such as cleaning of intricate or hard-to-reach parts, emulsification and homogenization of immiscible liquids, atomization of liquids or inks, particle agglomeration, degassing of liquids, catalysis of chemical reactions, machining, welding of plastics and metals, medical therapy and surgery, metal casting, dispersion of solids in liquids, and foam control (80-83). The underlying principle behind each of these processes can be related to cavitation effects, heat generation, mechanical effects, diffusion, stirring, and chemical effects. Of these effects, cavitation is perhaps the one that plays an integral role in most processes. As the sound wave propagates within the medium, individual particles are alternatively subjected to compression and refraction, although their relative positions do not change. For large sound wave amplitudes the magnitude of the negative pressure in the rarefaction areas, associated with the low-pressure half-cycle of vibration of the transducer, produces micron-size gaseous cavities to be formed. These cavitation bubbles grow until an unstable state is reached during the high-pressure half-cycle of operation, in which the bubbles collapse giving rise to huge pressure gradients as the liquid rushing from opposite sides of the bubble collides. The implosion event generates a microjet which impinges at high velocity on the surface to be cleaned. It has

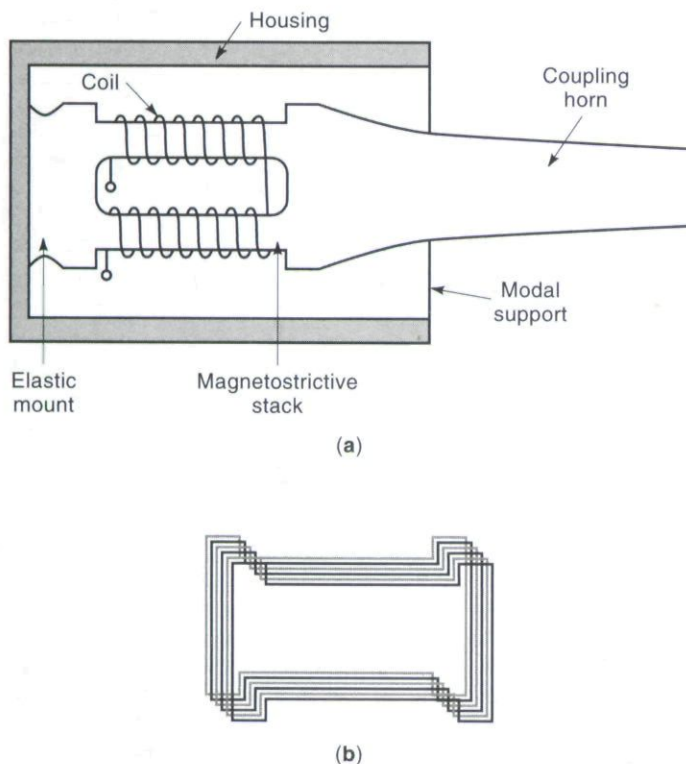


**Figure 18.** (a) Ultrasonic transducer with coupling exponential horn (79). (b) Detail of magnetostrictive stack. The stack can be attached (by silver brazing for instance) directly to the resonating diaphragm in the washing tank (79).

been calculated that locally the pressure rises to about 10 ksi, with an accompanying temperature rise of about 10,000 K (80). The combination of high speeds, pressure, and temperature, together with conventional cleaning agents, frees contaminants from their bonds with the surface.

Magnetostrictive transducers utilizing nickel as the active element are currently used for industrial cleaning and degassing of liquids, at operating frequencies of 20 kHz to 50 kHz (Blue Wave Ultrasonics, PMR Systems, Pillar Power Sonics). For dental and jewelry applications the operating frequencies exceed 50 kHz. Although piezoelectric transducers are sometimes preferred for megahertz-range ultrasonic generation, the ruggedness and durability of magnetostrictive devices constitutes a very desirable characteristic. In addition, magnetostrictive materials do not need to be repolarized when accidentally heated beyond the Curie point, as is the case with piezoelectrics.

Details on ultrasonic half- and quarter-wave prototype transducers using a GMPC (giant magnetostrictive powder composite) material can be found in Ref. 15. The half-wavelength unit was tested for liquid atomization, whereas the quarter-wavelength unit was used for ultrasonic washing and, when coupled to a 10:1 horn, for welding of plastics and cutting of wood.

Both nickel and PZT materials are "high- $Q$ " materials, i.e., their characteristic response exhibits a sharp peak at resonance, providing a very narrow range of frequencies over which the material is capable of transducing large amounts of energy. The output and efficiency decrease drastically at operating frequencies away from the fundamental resonant frequency. This effect can prove very limiting in applications where the system resonance is prone to varying, such as due to load changes. On the other hand, Terfenol-D is a low- $Q$  ( $Q \leq 20$ ) material and hence it overcomes much of the bandwidth limitations of nickel and PZTs. Hansen reports (81) current progress in Terfenol-driven ultrasonic transducers for surgical applications (348  $\mu\text{m}$  displacement at 1 MHz), and for degassing of liquids for the bottling industry. Ultrasonic welding and engraving using Terfenol are also being studied. A 15 kW, 20 kHz ultrasonic projector is currently being developed in an Etrema-NIST research effort (4). The projected areas of applicability of the device are devulcanization of rubber for recycling, catalysis of chemical reactions, and ultrasonic treatment of seeds to improve yield and germination efficiency.

Another field of high research and commercial interest is that of ultrasonic motors. The use of ultrasonic motors is being extensively explored in robotics, aerospace, automotive, and consumer applications. One visible example at the consumer level is the ring-type ultrasonic motor used for autofocusing camera lenses. Many kinds of ultrasonic motors have been developed, but two main categories can be distinguished (84): the vibrating driver type, and the progressive wave type. The vibrating driver uses the elliptical motion of a PZT driver, whereas the progressive wave motor uses the frictional force between the PZT driver and translator. Either type presents attractive features such as fine controllability, good efficiency, and compact size. However, the driving force is restricted by the friction generated between the moving surfaces, and most importantly, by the shearing strength of the PZT. To overcome these limitations, Akuta (74) developed a rotational actuator using Terfenol-D to achieve large am-

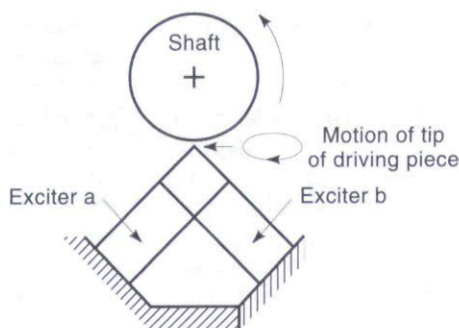


Figure 19. Terfenol-D ultrasonic rotational motor, after Akuta (74).

plitude elliptical vibrations, high torque, and fine angular controllability. The motor, illustrated in Fig. 19, has a speed of 13.1 rpm, and maximum torque of  $0.29 \text{ N} \cdot \text{m}$  at a rotational speed of 1300 Hz.

Recent research (85) indicates it is feasible to produce remotely powered and controlled standing wave ultrasonic motors (SWUMs) using thin film rare earth-iron alloys. The motor is completely wireless, and the excitation coil can be placed away from the active rotor. This represents a unique feature, not possible to achieve with piezoelectric technology, which can be used for intrabody distribution of medication, micropositioning of optical components, and actuation of small systems such as valves, electrical switches, and relays. A linear motor with these characteristics producing speeds of 10 to 20 mm/s and a rotational unit producing  $1.6 \mu\text{N} \cdot \text{m}$  of torque at 30 rpm were built.

#### Other Actuator Applications

We include a list of miscellaneous applications which take advantage of the large strains and force characteristics of magnetostrictive materials: wire bonding clamp for the semiconductor packaging industry (86); dexterous force reflection device for telemanipulation applications (87); hearing aid device based on the generation of low amplitude vibrations to bone, teeth, and similar hard tissue using Terfenol-D (88); magnetostrictive borehole seismic source (89); system for high-frequency, high-cycle fatigue testing of advanced materials using a magnetostrictive actuator (6,90); magnetostrictive fuel injection valve (15). An interesting review of some additional actuators is given by Restorff in Ref. 91.

#### MAGNETOSTRICTIVE SENSOR APPLICATIONS

The focus of this section will be magnetostrictive sensors, devices that rely on a material's magnetoelastic properties to convert a physical dimension into an electrical signal that can be processed and transmitted. The sensor system includes the sensor components themselves, the target, and supporting electronics. Some sensor systems use the inherent magnetoelastic properties of the target to effect the detection of the property of interest. For example, magnetoelastically induced elastic waves can be used to monitor a ferromagnetic specimen, such as pipes or the reinforcement bars (rebar) used in concrete structures. In other sensor configurations, the magnetostrictive properties of part of the sensor allow the measurement of the property of interest. In particular, we focus

on sensor designs and configurations that have some experimental verification.

#### SENSING EFFECTS

Magnetostrictive sensors can be divided into three groups based on how the magnetomechanical properties of the system components are used to measure the parameters of interest: (1) passive sensors, (2) active sensors, and (3) combined sensors. Passive sensors rely on the material's ability to change as a result of environmental stimuli to make measurements of interest. Passive sensors use the magnetomechanical effect such as the Villari effect to measure external load, force, pressure, vibration, and flow rates. Active sensors use an internal excitation of the magnetostrictive core to facilitate some measurement of core attributes that change in response to the external property of interest. For example, the magnetic permeability of Terfenol-D is sensitive to temperature. With proper calibration, temperature can be determined by measuring changes in the strain produced through excitation of a Terfenol-D sample with a known applied magnetic field.

Designs that employ two coils, one to excite the magnetostrictive component and one for measurement, are known as transformer-type sensors. The most common active sensor design mentioned in literature is the noncontact torque sensor. This employs variations on a general theme of using a magnetostrictive wire, thin film, or ribbon wrapped around or near the specimen that is subject to a torque. The change in the magnetic induction can then be related to the torque on the specimen.

Finally, combined sensors that use Terfenol-D as an active element to excite or change another material have been developed. They will allow measurement of the property of interest. For example, a fiber optic magnetic field sensor uses the change in length of a magnetostrictive element in the presence of a magnetic field to change the optical path length of a fiber optic sensor. There are numerous examples of combined sensors, including those to measure current, shock (percussion) and stress, frost, proximity, and touch. Stress can be measured using photoelastic material, and highly accurate displacement measurements can be made with the help of a magnetostrictive guide. Fiber optics and diode lasers have been used with magnetostrictive elements to measure magnetic flux density (magnetometers) (92). NDE (nondestructive evaluation) applications have also been developed, such as a corrosion sensor for surveying insulated pipes. Applications are discussed later in terms of the measured property or quantity: torque, magnetic field, material characterization, motion, force, and miscellaneous characteristics.

#### Torque Sensors

Torque measurement has great benefit in a variety of applications and industries, including the automotive industry and high-speed machining. Magnetostrictive torque sensors are traditionally based on the inverse magnetostrictive effect (Villari effect), where a torque-induced change in stress in the target causes a change in the magnetization of a magnetostrictive element in the sensor-target system. This change in magnetization can be measured directly (passive) or as a change in permeability with active excitation (active). A thorough overview of torque sensor technology, focusing on mag-

netostrictive torque sensors, is given in papers by Fleming (93).

**Noncontact Torque Sensors.** One of the most common torque sensor configurations is the noncontact torque sensor. The change in the stress in a ferromagnetic shaft is measured by detecting the change in permeability of a ferromagnetic element flux linked to the shaft. Figure 20 shows the basic design components, which include a C-shaped ferromagnetic core with an excitation and detection coil. Two variables in the sensor system are the excitation coil current  $I$  and the air gap between the shaft target and the sensor core. Noncontact torque sensors are advantageous because implementation is simple and fast. The performance is highly stable, accurate, and sensitive. Fleming investigated several issues with these sensors, including nonlinearities caused by sensor element properties, the effects of magnetic saturation, and excitation frequency (94).

**Thin-Film Torque Sensors.** An alternative torque sensor configuration is to apply the magnetostrictive material directly to the target. This idea was developed by Yamasaki, Mohri, and their collaborators, who used a wire explosion spraying technique to adhere thin layers of Ni, Fe-Ni, and Fe-Co-Ni to shafts (95). In this method, the conductive wire is exploded at a high temperature into fine particles that adhere strongly to the shaft. The wire explosion technique results in a sufficiently strong adhesion that they report increased sensor reliability relative to competing technologies that rely on epoxies to fix magnetostrictive material to a surface. When the shaft is twisted, stress in the film causes a change in its magnetization-applied magnetic field hysteresis loop. When two such regions of magnetostrictive material are surrounded by coils connected in a multivibrator bridge circuit (96) a change in voltage caused by a change in the torque can be detected. A linear, nonhysteretic relationship between the bridge circuit output voltage and the torque was obtained, with Ni and Fe<sub>42</sub>-Ni<sub>58</sub> providing the greatest sensitivity.

A second system using a 300  $\mu\text{m}$  thick Ni layer applied by plasma jet spraying was investigated by Sasada et al. (97). The instantaneous torque on a rotating shaft was related to

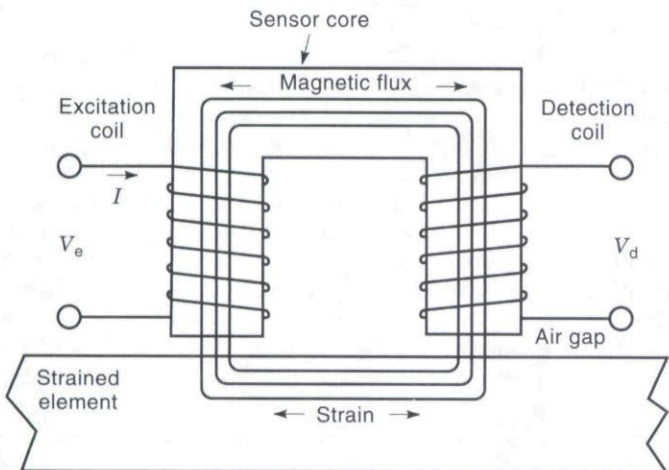


**Figure 20.** Noncontact torque sensor with excitation and detection coils around legs of C-shaped ferromagnetic core (32).

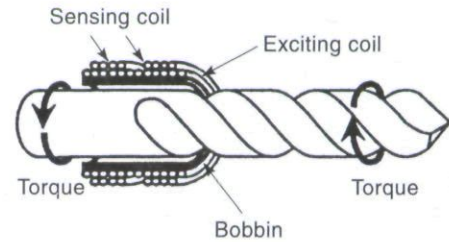


**Figure 21.** Noncontact measurement of torque on drill employing one excitation coil and two sensing coils one over the shank and one over the flutes (98) © IEEE 1994.

the magnetic circuit permeability measured using a pair of U-shaped magnetic heads positioned at  $\pm 45^\circ$  from the shaft axis. The sensitivity of the measurements to the air gap between the shaft and the magnetic heads was examined, and a self-compensating method was presented. A relatively linear sensitivity of 500 V/N · m with little hysteresis was measured. In addition, the output response of the sensor was found to be nearly independent of the rotational frequency.

**Sensor Shafts.** These applications are examples of taking advantage of the magnetostrictive effects of the target material itself. In the first example, the in-process detection of the working torque on a drill bit is related to the drill permeability. An excitation coil surrounds part of the drill including the shank and the flutes, as in Fig. 21 (98). Two sensing coils, one positioned over the flutes and one over the shank, are connected in series opposition allowing the measurement of the permeability. The permeability of the shank is less sensitive to changes in torque than the flutes, and the difference in the output voltages of the two coils changes in proportion to the applied torque. In the second example, a sensor shaft was made of Cr-Mo steel suitable for automobile transmission applications. Two grooved sections are surrounded by coils, which are configured in an ac bridge circuit. When torque is applied to the shaft, the Villari effect results in a change in impedance measured by the bridge. According to Shimada et al., this sensor design is robust with respect to temperature (99).

## Motion Sensors

**Bidirectional Magnetostrictive Transducers.** The existence of the Villari effects makes it possible for a magnetostrictive transducer, such as those described in the sonar and motion/force device sections to have two modes of operation, transferring magnetic energy to mechanical energy (actuation) and transferring mechanical energy to magnetic energy (sensing). As with many other transducer technologies such as electromagnetic (moving coils) and piezoelectricity, magnetostrictive transduction is reciprocal, and a transducer has the ability to both actuate and sense simultaneously. Applications such as the telephone and scanning sonar use this dual mode. For example, Terfenol-D sonar transducers can be used as either a transmitter or receiver or both at the same time. Another potential use of dual-mode operation is in active vibration and noise control. One transducer can be used to sense deleterious structural vibrations and provide the actuation force to suppress them. This approach to active control provides what is called colocated sensing and actuation, which aids in ensuring

control system stability. Self-sensing control uses the sensed signal in a feedback loop to drive the transducer. Numerous papers have described systems based on this effect and shown its effectiveness (66,100,101).

Fenn and Gerver have developed, tested, and modeled a velocity sensor based on a permanent magnet biased Terfenol-D actuator (102). The output from the device was a voltage induced in a coil surrounding the monolithic Terfenol-D core, which was proportional to the time rate of change of the strain in the Terfenol-D core and ultimately the velocity of the connected target. Peak sensitivities of 183 V/m/s were seen when the coil was left open. In addition, the coil could be shunted to provide passive damping capability, and the voltage proportional to the target velocity could be monitored across the shunt resistor.

**Noncontact Magnetostrictive Strain Sensors.** Noncontact magnetostrictive strain sensors (NMASSs) use the magnetic field to couple the straining target to the sensing element. A noncontact system has several advantages (103). First, it is a noninvasive technique; that is, it does not require mechanical bonding to the target. This is a significant advantage for measuring strain of rotating targets. Second, the sensor can be moved to measure strain at different points easily and quickly, perhaps providing a three-dimensional strain-mapping capability. Finally, this sensor is rugged, with good sensitivity and overload capacity. Figure 20 shows the general configuration of the sensor (103) with the C-shaped ferromagnetic sensor core wound with an excitation and sensing coil. The flux path crosses the air gap to the target. Because of the magnetoelastic effect, strain in the target causes a change in the magnetic circuit permeability, which will be seen as a change in the sensed voltage. In general, the sensor will detect changes in strain of ferromagnetic materials; however, strains in nonferromagnetic materials can be detected by applying a ferromagnetic layer on the surface. This sensor configuration has also been used to measure torque in shafts because the principal strains are  $45^\circ$  from the shaft axis.

**Magnetostrictive Waveguide Position Sensors.** The magnetostrictive waveguide position sensors detect the position of a permanent magnet connected to the target, which is free to move along the length of a magnetostrictive waveguide. An emitter is used to send a current pulse continuously through the waveguide, which produces a circumferential magnetic field. This combined with the longitudinal magnetic field produced by the permanent magnet results in a helical magnetic field.

The Wiedemann effect described earlier then results in a torsional strain pulse; the triggered torsional acoustic wave travels at the speed of sound in both direction away from the permanent magnet along the waveguide. One end of the waveguide is fitted with a receiver; at the other end a damper attenuates the acoustic wave so that it will not reflect back corrupting the signal at the receiver and avoiding the development of standing waves. The receiver measures the time lapse between the current pulse and the acoustic wave, which is related to the distance between the receiver and the permanent magnetic/target. The acoustic wave can be measured by the change in permeability resulting from the strain pulse in

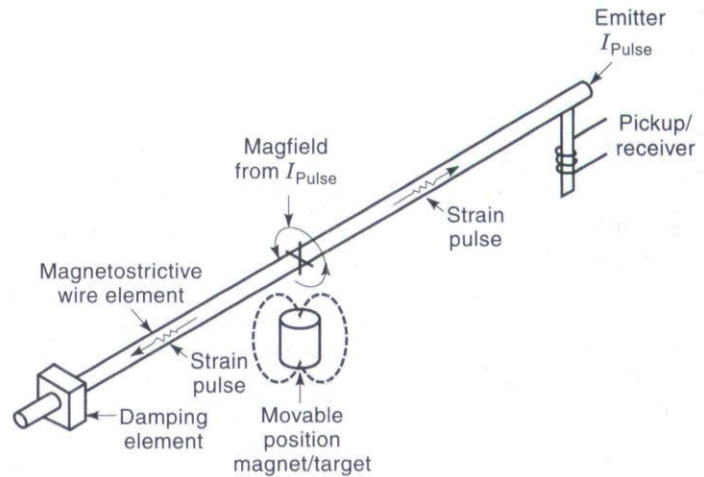


Figure 22. Magnetostrictive waveguide position sensor (93).

the waveguide. In Fig. 22, the receiver, or pick-up element, is shown as a magnetostrictive ribbon welded to the waveguide that converts the torsional pulse to a longitudinal elastic pulse. The permeability of the ribbon, which changes as a result of the elastic pulse, is monitored via Faraday's Law with a coil wrapped around the ribbon. A piezoelectric element can also be used as the receiver to measure the acoustic wave.

Several versions of this sensor are available commercially and discussed in the literature. Nyce describes the operation of MTS model LP in detail (104). Current pulses with frequencies between 10 Hz and 10 kHz provide the excitation. The sensor performance is considered as a function of the magnetostrictive waveguide material (high magnetostriction, low attenuation, and temperature stability are desired), and geometry. Lucas Control System Products (United Kingdom and United States) has developed the MagneRule Plus, a compact position sensor for measurements up to 120 in. (305 cm) with high linearity and repeatability. In addition, it can measure fluid levels by connecting the permanent magnet to a float, which is then placed in the fluid to be monitored. Finally, Equipel (France) manufactures and sells Captosonic position sensors capable of measuring distances up to 50 m with  $\pm 1$  mm accuracy (105).

**Magnetoelastic Strain Gages.** Using the fact that the permeability of many magnetostrictive materials is stress sensitive, a strain gage made from strips of Metglass 2605SC has been developed by Wun-Fogle and associates (106). The permeability of the ribbons decreased in tension and increased in compression. The ribbons were prepared by annealing in a transverse 2.6 kOe magnetic field at  $390^\circ\text{C}$  for 10 min and then rapidly cooled in a saturation magnetic field. To maintain their high sensitivity, the ribbons must be strongly bonded to the target in an initially stress-free condition. A highly viscous liquid bond was found to bond the ribbons to the target adequately, although it did result in a loss of dc response. For experimental verification, two ribbons were placed on the top and bottom of a beam and surrounded by two coils connected in opposition. The ribbons were excited by an external magnetic field of 1 kHz. The net voltage in the coil system was related to changes in permeability and, hence, changes in

strain of the ribbons. The strain measurement system resulted in a figure of merit, given by  $F_{\mu} = (\partial\mu/\partial\epsilon)/\mu$ , of  $4 \times 10^5$  which compares favorably with conventional strain gages. It was found that strains on the order of  $10^{-9}$  could be measured at 0.05 Hz.

**Magnetostrictive Delay Lines (MDLs).** An acoustic pulse is propagated through the magnetostrictive delay line and detected by a receiving unit. A current pulse through a conductor (PCC) orthogonal to the magnetostrictive delay line (MDL) generates a pulsed magnetic field in the MDL, which generates an elastic wave, see Fig. 23. An active core (AC) of soft magnetic material, placed near the PCC, is connected to the target and is free to move relative to the MDL. The magnetic pulse and hence elastic wave generated in the MDL is sensitive to the magnetic coupling between the AC and MDL. As the target and AC move away from the MDL, the magnetic coupling between the PCC and MDL increases so that the magnetic pulse and elastic wave in the MDL increases in strength. The output to the sensor is the pulse generated in the receiving unit coil (RC) as described by Faraday's Law. The output voltage induced in the RC is sensitive to the gap distance between the MDL and AC; for MDL-AC, displacement is less than 2 mm. Most importantly, the output is fairly linear and anhysteretic with respect to the MDL-AC displacement. Sensitivities of  $10 \mu\text{V}/\mu\text{m}$  have been reported using 24- $\mu\text{m}$  thick Metglas 2605SC amorphous ribbon as the MDL (79). Permanent magnets were also used to maximize the generation of the acoustic pulse and the measured voltage in the RC. Multiple AC-PCC elements can be used with one MDL to form an integrated array. This novel aspect of the sensor system and several AC-PCC-MDL configurations are discussed by Hristoforou and Reilly (107). Applications for this sensor include tactile arrays, digitizers, and structural deformations.

**Force Sensors**

**Magnetostrictive Delay Lines.** The magnetostrictive delay line displacement sensor configuration has been modified to produce a force distribution sensor (108,109). A force applied directly to the MDL will distort the acoustic signal by the emitter as described previously. The change in the acoustic wave measured by a receiver coil is related to the force applied to the delay line. An experimental device tested by Hristoforou and Reilly (108) used a Metglas 2605SC FeSiBC amorphous ribbon as the delay line embedded in a fiberglass channel. The channel bends under an applied force, stressing

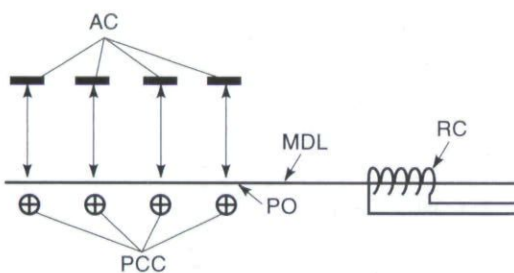


**Figure 23.** Magnetostrictive delay line with active core connected to target, pulsed current conductor, receiving coil, and point of origin (PO) for acoustic stress (79) © IEEE 1994.

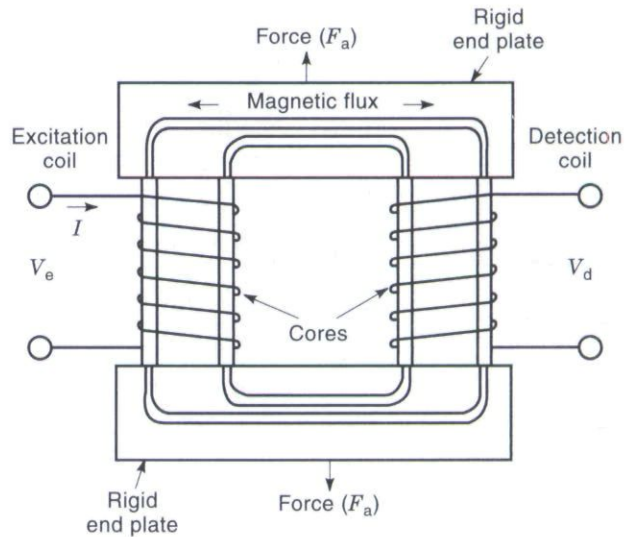


**Figure 24.** Magnetostrictive sensor for measuring force, composed of two ferromagnetic cores, one with an excitation coil and the other with a sensing coil, between two rigid end plates (85).

the MDL. In addition, the channel ensures that the PCC oriented perpendicular to the MDL ribbon on the bottom of the channel does not move relative to the MDL. For a given current, the voltage detected by the receiver coil caused by a force  $F$  is proportional to the  $e^{-cF}$ , with calibration constant  $c$ . Integrated arrays for measuring force can be constructed with multiple MDL (each with a receiver) and PCC oriented perpendicularly. The values of multiple forces on the two-dimensional array can be backed out from the voltages measured by the receivers.

**Magnetostrictive Force Sensor.** Kleinke and Uras describe a force sensor that employs the change in electrical impedance of a coil that is flux linked to a magnetic circuit to measure the stress or force acting on a magnetostrictive component in the magnetic circuit (110). It is similar in construction to the noncontact magnetostrictive strain sensor discussed earlier. However, rather than having a C shape, two magnetostrictive cores are held in place by rigid end pieces, see Fig. 24. A coil surrounds each core, one of which is used for excitation and the other for sensing. A constant amplitude ac is impressed in the excitation coil generating an oscillating magnetic field. This results in a voltage in the detection coil with a magnitude proportional to the time rate of change of flux linking the detection coil. An applied force on the sensor will cause a strain change in the magnetostrictive cores resulting in a change in the core magnetization. In this mode, where the magnetomotive force is kept constant, a change in the output voltage from the detection coil is linearly related to the change in force. In a constant flux operation mode, the excitation current is allowed to vary in order to maintain a constant detection coil output voltage. In this case the change in excitation current is related to the change in force. Compared with conventional force transducers such as those that employ strain gages, this force sensor is simpler, more rugged, relatively inexpensive, and employs simpler electronics.

**Amorphous Ribbon Sensors.** A tensile force sensor based on the strong Villari effect of amorphous ribbons, such as Ni,

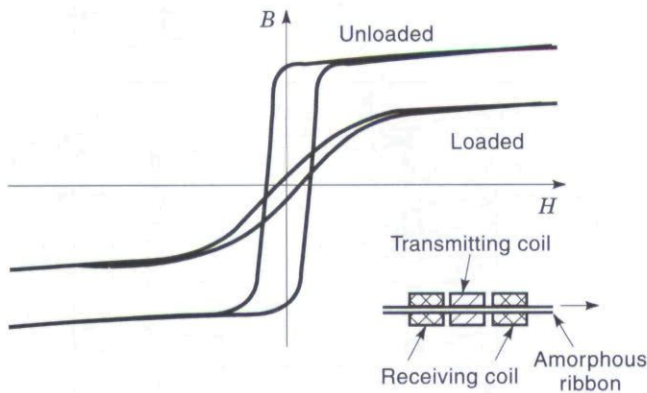


**Figure 25.** Amorphous ribbon force sensor with one excitation coil and two receiving coils so that changes in permeability caused by a force are detected (129).

Fe-, and Co-based alloys, has been described by Seekircher and Hoffman (111). A transmitting coil excites the ribbon while a pair of detection coils measure the maximum induction, which is dependent on the stress as shown in Fig. 25. Loads below 4 N were measured with Co alloy ribbon, 25  $\mu\text{m}$  thick by 3 mm wide with negligible hysteresis. The high Young's modulus of the ribbons results in low-displacement sensors, which can be load-bearing elements. In some cases, temperature compensation is required.

Numerous torque sensor designs, patents, and literature are also available. Highly sensitive shock-stress sensors employing iron-rich amorphous ribbons are described in detail by Mohri and Takeuchi (112). A combined torque-force sensor has also been developed (113). The change in permeability (or magnetic flux) in a magnetic circuit resulting from strain in an element of the circuit can be used to measure both torque as described previously and force.

#### Material Characterization Magnetostrictive Sensor

Figure 26 shows a noncontact sensor that uses the magnetostrictive properties of the target material to excite elastic waves that can be measured and monitored for use in characterizing the target material properties (114–116). The system can be used only with ferromagnetic material that has a magnetoelastic response. The sensor consists of a transmitting coil (pulse generator, power amplifier, and bias magnet) surrounding the object, which generates the mechanical wave via

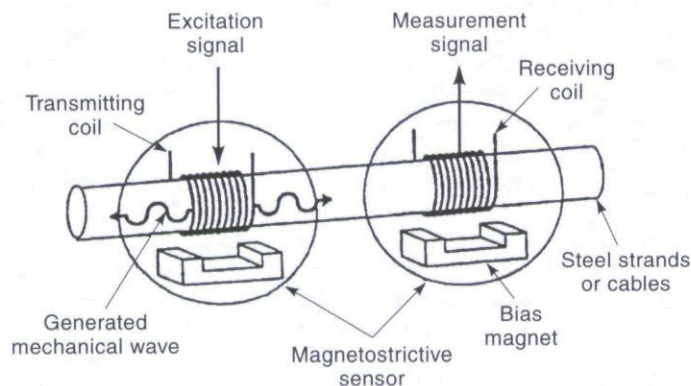


**Figure 26.** Magnetostrictive sensor for characterizing corrosion and monitoring ferromagnetic materials such as pipes and strands (130).

magnetostrictive excitation. A receiving coil (signal preamplifier, data acquisition hardware, and permanent magnet) located at a distance from the excitation coil measures the signal produced by the waves. These signals can be used to characterize the material for corrosion, measure stress in strands, and so on. Signals are generated by changes in the material geometry. Experimentation has shown that the wave attenuation increases with the degree of corrosion. This method has been used successfully to identify corrosion in strands, reinforced bars (including those embedded in cement), water pipes, and other systems where noninvasive monitoring techniques are preferred.

#### Magnetometer

There are numerous designs for magnetic field sensors, including many which rely on magnetostrictive properties of component materials. These sensors vary considerably, in part because they are designed to detect magnetic fields of different strengths and frequencies (117).

The first magnetometer design, developed by Chung et al., employs a Terfenol-D sample to convert a magnetic field into a measurable quantity (118–120). A Terfenol-D rod strains in the presence of an ac magnetic field. This displacement can be measured accurately with a laser interferometer calibrated to output a signal related to the magnetic field. A dc magnetic bias is used to optimize the sensitivity of the Terfenol-D strain with magnetic field, resulting in values of up to 10  $\mu\text{L}/\text{L}/\text{gauss}$ . In addition, the sensitivity was found to be a function of the mechanical prestress.

Other magnetic field sensors are also available. In 1979 Yariv and Winsor proposed a now common configuration that uses a magnetostrictive film coating applied to an optic fiber (121). The magnetic field causes the magnetostrictive film to deform, straining the optic fiber. This causes changes in the optical path length and the phase of the laser light passing through the optic fiber, which can be detected by an interferometer. Mermelstein shows that the resolution limit at dc to low frequency (less than 1 Hz) of such a sensor is approximately  $3 \times 10^{-11}$  Oe (122). Magnetostrictive amorphous metals, often in the form of ribbons, are extremely sensitive to external magnetic fields and have been used as the active element of a magnetometer (96). Finally, a magnetic field sensor has been developed based on magnetostrictive delay line technology (123).

#### Miscellaneous

Magnetostrictive sensors have been used to measure or monitor a number of other properties and characteristics. Some examples found in the literature include hearing aids (88), magnetoelastic delay line digitizers (124), magnetoacoustic keyboards (125), thermometers (126), biomedical monitors for lung ventilation (127) and spine movement (128), bimorphs for two-dimensional scanning elements (129), and composite cure monitors. An interesting review of additional sensors is given by Restorff in Ref. 91.

#### MAGNETOSTRICTIVE DEVICE MODELING

The increased use of magnetostrictive materials has not been accompanied by the availability of complete and accurate

transducer models. Complete models must incorporate the different operating regimes present in magnetostrictive transducers in a manner compatible with the requirements of specific applications. The regimes present in magnetostrictive transducers are electric (which involves routing of magnetic field through magnetic circuit for magnetization of the magnetostrictive core), mechanical (elastic state of the materials present in the transducer), and thermal (the temperature distribution in the transducer materials). Extensive experimental evidence (21,28,31) demonstrates that it is crucial to consider the interaction between these regimes; therefore, models for the various regimes need to be coupled to provide a complete description of a transducer system.

Most of the currently available models of magnetostrictive transducers fail to incorporate all regimes simultaneously. This is in part because transducer models are still predominantly based on the linear constitutive piezomagnetic equations [Eq. (1)] (14). These equations neglect the effects of coupling between stress, magnetization, and temperature in the material, which have a bearing on the mechanical performance as indicated in Ref. 35, among others.

Carman and Mitrovic (130) and Kannan and Dasgupta (131) extended the scope of the linear constitutive equations by including specific nonlinear effects. The nonlinear dynamics of magnetostrictive transducers has been also modeled following a phenomenological approach. One such approach is obtained through the use of generalized Preisach operators. Preisach models that specifically target giant magnetostrictive materials are discussed by Restorff et al. (132), Adly and Mayergoyz (133), and Smith (134). These models characterize different operating regimes but are cumbersome to implement in magnetostrictive transducers where performance changes significantly during operation.

Other modeling efforts have combined physical laws with phenomenological observation. Engdahl and Berqvist (135) present a model capable of dealing with nonlinearities and various losses, such as magnetomechanical hysteresis, eddy currents, ohmic heating, and mechanical losses. Physically based Preisach models combined the empirical robustness of nonphysical laws with some understanding of the physical processes that govern magnetic and magnetostrictive hysteresis. Basso and Bertotti (136), for instance, developed a Preisach-based hysteresis model for materials where the magnetization is dominated by domain wall motion.

Nevertheless, there does not exist a fundamental model applicable to the complete performance space of magnetostrictive transducers. The development of physics-based models that incorporate the different operating regimes and the issues inherent to them will certainly extend the utility of these transducers. In this section, some of the fundamental issues in magnetostrictive transducer modeling are identified, and some of the current state-of-the-art modeling techniques that handle these different issues are reviewed.

### Linear Transduction

The linear transduction equations provide a "black box" model of the relationship between electrical and mechanical sides of the transducer through the transducer's total electrical impedance. These equations can be written

$$V = Z_e I + T_{em} v \quad (14a)$$

$$F = T_{me} I + z_m v \quad (14b)$$

where  $V$  and  $I$  are voltage and current across transducer leads,  $Z_e$  is the blocked electrical impedance,  $v$  is velocity,  $T_{em}$  and  $T_{me}$  are electrical due to mechanical and the mechanical due to electrical transduction coefficients, and  $z_m$  is mechanical impedance. Hunt, Rossi, and many others have authored authoritative texts on the subject of transduction covering the use of equivalent circuit models such as that presented in Fig. 8(b) and the transduction equations as applied to modeling of magnetostrictive devices.

### Magnetization

Magnetization and the magnetoelastic interactions taking place inside the magnetostrictive core and other transducer components have been modeled in different manners. Transducer magnetic models can be formulated using standard techniques (see MAGNETIC CIRCUITS) (i.e., using equivalent circuit representations and/or finite element modeling approaches). The least well-defined component of such models is inevitably the magnetic state of the magnetostrictive core, which, referring back to Fig. 3, changes significantly with operating conditions.

One approach for modeling a magnetostrictive material is to consider the material at its micromagnetics level. Classical micromagnetics work by Brown (137) assumes that the material is simultaneously magnetizable and deformable with its energy state defined by elasticity, thermodynamics, and electromagnetic principles. Recent work in this field deals specifically with Terfenol-D (138). Although the modeling results are useful at the domain level, the extension of micromagnetic models to describe the performance of transducers is a major undertaking.

The Preisach model has been used extensively for characterization of ferromagnetic materials, and more recently for characterization of magnetostrictives as well. Much research effort has been devoted to accommodate physical aspects into the Preisach approach, which in its original form, cannot be traced back to fundamental principles. Reimers and Della Torre implement in Ref. 139 a fast inverse hysteresis model amenable to control applications and with applicability to magnetostrictive materials.

Following the classical anisotropy domain rotation model by Stoner and Wohlfarth (140), Lee and Bishop (141) extended their idea to a random assembly of domain particles having cubic anisotropy. Clark et al. (142) included compressive loading along the [111] easy axis direction in a two-dimensional scheme. Jiles and Thoenke (143) generalized this model to three dimensions, by considering the anisotropy, magnetoelastic, and field energies along all three directions. Although model results are in good agreement with measured data, the identification of the fractional occupancies, which define the participation of different easy axes in the total magnetization, is by no means trivial.

Another modeling approach that yields significant results is the ferromagnetic hysteresis model. Theory by Jiles and Atherton (144) predicts quasi-static magnetization-applied field ( $M-H$ ) loops in ferromagnetic materials by considering the energy of domain walls as they bow and translate during magnetization. Later extensions include models of magnetostriction, eddy current losses, minor loops, and mechanical prestress (see Ref. 39). The appeal of the Jiles-Atherton model stems from the physical basis of the model parameters and the fact that only five parameters are needed for complete

description of the magnetic state of the material. However, this model is purely magnetic in nature, which highlights the need for accurate and general magnetomechanical characterization laws to describe the transduction process in the transducer completely.

### Stress

It is common practice to place giant magnetostrictive samples under a mechanical compressive prestress for operation. The ability of the material to survive high accelerations and shock conditions improves under compressive stress because, for example, Terfenol-D is much more brittle in tension (tensile strength  $\approx 28$  MPa) than in compression (compressive strength  $\approx 700$  MPa) (32). Under dynamic operating conditions in systems using the more brittle magnetostrictives such as monolithic Terfenol-D, the rated system output force is usually limited by the magnitude of the device prestress according to Newton's Second Law, where  $F = ma = \sigma_v A$ . Above the prestress, the output dynamic load will accelerate away from the magnetostrictive driver, only to return with potentially damaging results. In addition, adequate preloading is capable of improving the magnetic state in the material as a consequence of the coupling between the magnetic and mechanical states. Figure 9(c) shows transducer electrical impedance function sensitivity to changes in prestress.

Considering an energy balance in the material, the mechanical prestress is an additional source of anisotropy energy that competes against the magnetocrystalline anisotropy, strain, and applied field energies. The application of the compressive preload forces a larger population of magnetization vectors to align perpendicular to the direction of application of the preload, where a state of local minimum energy is reached. This translates into both a smaller demagnetized length and increased saturation magnetostriction. However, for compressive preloads larger than a certain value, the prestress energy overpowers the elastic energy produced by the material and the magnetostriction decreases.

The relationship  $\epsilon$ - $M$  in Terfenol-D has been reported to be nearly independent of prestress except for very low prestresses and high magnetizations. Clark et al. (145) report a range of about 15 MPa to 55 MPa for the  $\epsilon$ - $M$  stress independence in Bridgman-grown samples. In addition, work by Kvarnsjö (146) indicates that at high prestresses, the primary magnetization mechanism is domain magnetization rotation; as a consequence, the quadratic law for magnetostriction discussed earlier is appropriate. Clark et al. (145) found that the quadratic law is incorrect in the low prestress regime (below 30 MPa for statically loaded, single-crystal material) where it was found that strain depends directly on stress and that the magnetostriction cannot be accounted for by a single-valued magnetization law (i.e., hysteresis is observed).

### Thermal Effects

Temperature effects can be incorporated in the linear piezomagnetic model given in Eq. (1). Furthermore, by considering higher-order interactions between magnetization, stress, and temperature, Carman and Mitovic (130) developed a model capable of producing results in good agreement with experimental data at high preloads. However, the model is not capable of predicting saturation effects. Following the lead of Hom and Shankar (147), Duenas, Hsu, and Carman (14) developed

an analogous set of constitutive equations for magnetostriction. These equations are given by

$$\epsilon_{ij} = s_{ijkl}^M T \sigma_{kl} + Q_{ijkl}^T M_k M_l + \alpha_{ij}^M \Delta T \quad (15a)$$

$$H_k = -2Q_{ijkl}^T M_l \sigma_{ij} + \frac{M_k}{k|M|} \operatorname{arctanh}\left(\frac{|M|}{M_s}\right) + P_k^T \Delta T \quad (15b)$$

where  $\epsilon$  is strain,  $s$  is compliance,  $Q$  is the magnetostrictive parameter,  $M$  and  $M_s$  are magnetization and saturation magnetization,  $\alpha$  is coefficient of thermal expansion,  $T$  is temperature,  $H$  is magnetic field,  $P$  is the pyromagnetic coefficient, and  $k$  is a constant. Superscripts indicate the constant physical condition under which the parameter is measured, and subscripts indicate tensor order following conventional notation. This model successfully captures the quadratic nature of magnetostriction for low to medium field levels, but it does not completely describe the saturation characteristics. The model allows the incorporation of magnetostrictive hysteresis via complex model parameters.

Heat not only affects the magnetization processes in the magnetostrictive core but also has bearing on the overall transducer design. Together with magnetomechanical hysteresis and eddy current losses, ohmic heating in the excitation coil is perhaps one of the most significant sources of losses. Other thermal effects to consider in transducer design are thermal expansion of the magnetostrictive driver itself [for Terfenol-D,  $\alpha \approx 12 \times 10^{-6}/^\circ\text{C}$  (32)], dependence of material properties and performance of Terfenol-D on temperature, thermal expansion of the coil (coils used in prototype transducers showed expansion above 1.5% when heated from room temperature to temperatures of around  $100^\circ\text{C}$ ), thermal expansion of other transducer components, and the thermal range of the coil insulation. Maintaining controlled temperatures during operation is critical for certain transducer applications. One clear example of this is precision machining. Transducers for this type of application need to use efficient thermal sinks, either active (cooling fluids), passive (thermally conducting materials, superconducting solenoids), or a combination of the two.

### Ac or Eddy Current Losses

Dynamic operation leads to additional complications in the performance of magnetostrictive transducers. One important loss factor to consider is the eddy (or Foucault) currents. As modeled by the Faraday-Lenz Law, eddy currents are set up in the transducer's conducting materials to resist magnetic flux changes. These currents produce a magnetic flux that resists the externally applied magnetic field and simultaneously cause a nonuniform distribution of current density often known as skin effect.

Classical eddy current power loss formulations assume complete magnetic flux penetration and homogeneous permeability throughout the material. This assumption is valid only for small material thickness (e.g., laminas); hence, it is invalid for solid, thick cylindrical transducer cores. The characteristic frequency above which the homogeneity of penetration of the magnetic flux is compromised, for cylindrical samples, is given by

$$f_c = \frac{2\rho}{\pi D^2 \mu \epsilon} \quad (16)$$

where  $\rho$  is the resistivity of the material [ $\rho \approx 0.6 \times 10^{-6} \Omega \cdot \text{m}$  for Terfenol-D (120)],  $D$  is the rod diameter, and  $\mu^e$  is the clamped permeability. For a 6.35 mm (0.25 in.) diameter rod, the characteristic frequency is about 5 kHz. Laminations in the magnetostrictive core, low operating frequencies, silicon steel end caps, and slit permanent magnets help to mitigate the effects of eddy currents.

A modeling approach based on energy considerations is shown by Jiles (148). This approach considers eddy currents as a perturbation to the quasi-static hysteresis. The simplicity of this model is, however, offset by the limitations imposed by its assumptions. Because uniform flux penetration is assumed, its applicability is limited to thinly laminated material or low operating frequencies.

Another classical approach to the eddy currents issue is the one presented by Bozorth (9) among others. In this model, a so-called eddy current factor  $X$  is used to account for the reduced inductance caused by the oppositely induced magnetic field. The complex quantity  $X = X_r + jX_i$  can be written for cylindrical current-carrying conductors in terms of Kelvin ber and bei functions and is dependent upon frequency of operation  $f$  and the characteristic frequency  $f_c$  as follows:

$$X_r = \frac{2}{\sqrt{p}} \left( \frac{\text{ber } \sqrt{p} \text{ bei}' \sqrt{p} - \text{bei } \sqrt{p} \text{ ber}' \sqrt{p}}{\text{ber}^2 \sqrt{p} + \text{bei}^2 \sqrt{p}} \right) \quad (17a)$$

$$X_i = \frac{2}{\sqrt{p}} \left( \frac{\text{ber } \sqrt{p} \text{ ber}' \sqrt{p} - \text{bei } \sqrt{p} \text{ bei}' \sqrt{p}}{\text{ber}^2 \sqrt{p} + \text{bei}^2 \sqrt{p}} \right) \quad (17b)$$

where  $p = f/f_c$  is a dimensionless frequency parameter. An alternative, simpler presentation of the same formulation is shown by Butler and Lizza in Ref. 149.

### Dynamic Effects

As can be seen in Figs. 9(b,c), the resonant frequency of a Terfenol-D transducer varies significantly with operating conditions. The transducer mechanical resonance varies as a result of a number of factors. Some of these factors are the magnetostrictive core geometry, bias condition, delta  $E$  effect, ac magnetic field, external load, springs stiffness, and operating temperature. Other factors intrinsic to the specific design such as damping of internal components can also be significant.

The first mode axial resonance  $f_0$  of a Terfenol-D transducer such as that sketched in Fig. 1 is given by

$$f_0 = \frac{1}{2\pi} \sqrt{\frac{k_m + k_{ps}}{m_{\text{eff}}}} \quad (18)$$

where  $k_m$  is the magnetostrictive core stiffness given by Eq. (5),  $k_{ps}$  is the prestress mechanism stiffness, and  $m_{\text{eff}}$  is the system effective dynamic mass. The effective mass in the equation is formed by one-third of the mass of the rod plus the external load plus components of the prestress mechanism. Recognizing that the magnetostrictive material's compliance is strongly dependent upon operating conditions, the resonance frequencies of the device will be strongly dependent on operating conditions. Increasing ac magnetic field intensity increases the system compliance; hence, it decreases transducer resonant frequencies [Fig. 9(b)], while increasing prestress increases the system stiffness and hence resonant fre-

quencies [Fig. 9(c)]. Control of the transducer resonant frequency over a range of 1200 Hz to 1800 Hz using the delta  $E$  effect has been used in design of magnetostrictive moving-resonance or tunable vibration absorbers (150).

The dynamics of Terfenol-D transducers coupled to external loads are studied in Ref. 151. An in-plane force-balancing model is used to consider both passive forces (those associated with the transducer and external load structural dynamics) and active forces (derived from the magnetostriction effect) to yield a PDE (partial differential equation) transducer model. The active component of the force is characterized by the strains predicted by the Jiles–Atherton ferromagnetic hysteresis model, combined with a magnetostriction quadratic law. The passive component is characterized by a PDE model of the transducer and external load structural mechanics. The model is capable of predicting the quasi-static magnetization state of the transducer core, and of accurately predicting strains and displacements output by the transducer. The parameter requirements of this model are minimal [experimental identification of six physically based parameters from quasi-static hysteresis loop measurements (e.g., saturation strain and magnetization)] and the model is computationally nondemanding given the relative simplicity of the underlying PDE system. Work is in progress to incorporate the effects of ac losses.

### CONCLUDING REMARKS

The high strains and forces achievable with magnetostrictive transducers, high-coupling coefficients, and high-energy density of magnetostrictive materials have justified their use in an ever-increasing number of sensor and actuator applications, ranging from sonar projectors to vibration control, ultrasonics, and sensors designed to find corrosion in pipes. Magnetostrictive device performance capabilities are sometimes overlooked in the interest of avoiding nonlinear and hysteretic input–output transducer behaviors. The unique electromagnetomechanical coupling that takes place in these devices poses rigorous engineering challenges to those who would undertake magnetostrictive transducer design. As evidenced by the resurgence in patented devices based on magnetostriction, designers continue to overcome these challenges and make advances in modeling and controlling magnetostrictive device performance attributes. Furthermore, shrewd transducer designers are recognizing that many of these unique nonlinear behaviors afford the engineer who understands the material attributes a uniquely rich performance space. As material advances continue, it is expected that magnetostrictive device design engineers will find new magnetostrictive solutions to an ever-growing variety of transducer applications.

### BIBLIOGRAPHY

1. E. Lee, Magnetostriction and magnetomechanical effects, *Rep. Prog. Phys.*, **18**: 184–229, 1955.
2. E. du Tremolet de Lacheisserie, *Magnetostriction Theory and Applications of Magnetoelasticity*, Boca Raton, FL: CRC Press, 1993.
3. F. V. Hunt, *Electroacoustics: The Analysis of Transduction, and its Historical Background*, Amer. Inst. Phys. Acoust. Soc. Amer., 1982.

4. Nist Advanced Technol. Program, *Terfenol-D high power ultrasonic transducer*, Nist Grant No. 97-01-0023.
5. M. Moffett, R. Porzio, and G. Bernier, High-power Terfenol-D flextensional transducer, *NUWC-NPT Tech. Doc.*, **10**: 883-A, 1995.
6. G. Hartman and J. Sebastian, Magnetostrictive system for high-frequency high-cycle fatigue testing, Univ. Dayton Res. Inst., UDR-TR-97-116, 1997.
7. A. E. Clark and H. S. Belson, Giant room-temperature magnetostrictions in  $TbFe_2$  and  $DyFe_2$ , *Phys. Rev. B*, **5**: 3642–3644, 1972.
8. N. C. Koon, A. I. Schindler, and F. L. Carter, Giant magnetostriction in cubic rare earth-iron compounds of the type  $RFe_2$ , *Phys. Lett.*, **37A**: 413–414, 1971.
9. R. M. Bozorth, *Ferromagnetism*, Princeton, NJ: Van Nostrand, 1968.
10. J. L. Butler, *Magnetostrictive transducer design and analysis*, Image Acoustics, Inc., short course notes, Aug. 1997.
11. Y. Lu and A. Nathan, Metglass thin film with as-deposited domain alignment for smart sensor and actuator applications, *Appl. Phys. Lett.*, **70** (4): 526–528, 1997.
12. C. Body et al., Finite element modeling of a magnetostrictive micromembrane, *Proc. Actuator '96, 5th Int. Conf. New Actuators*, VTI-VDE, Bremen, Germany, 1996, pp. 308–311.
13. H. Uchida et al., Effects of the preparation method and condition on the magnetic and giant magnetostrictive properties of the  $(Tb,Dy)Fe_2$  thin films, *Proc. Actuator 96, Intern. Conf. New Actuators*, VDI-VDE, Bremen, Germany 1996, pp. 275–278.
14. T. A. Duenas, L. Hsu, and G. P. Carman, Magnetostrictive composite material systems analytical/experimental, *Symp. Advances Smart Materials-Fundamentals Applications*, Boston, MA, 1996.
15. T. Cedell, Magnetostrictive materials and selected applications. Magnetoelastically induced vibrations in manufacturing processes, Dissertation, Lund Univ., Sweden, 1995.
16. Y. Wu and M. Appa, Modeling of embedded magnetostrictive particulate actuators, *Proc. Symp. Smart Structures Materials*, Vol. 2717, 1996, pp. 517–529.
17. P. P. Pulvirenti et al., Enhancement of the piezomagnetic response of highly magnetostrictive rare earth-iron alloys at kHz frequencies, *J. Appl. Phys.*, **79**: 6219–6221, 1996.
18. M. Wun-Fugle et al., Hysteresis reduction and magnetostriction of dendritic  $[112] Tb_xDy_yHo_zFe_{1.95}$  ( $x+y+z=1$ ) rods under compressive stress, 1998 *ONR Transducer Materials Transducers Workshop Proc.*, May 1998.
19. R. James and M. Wuttig, Ferromagnetic shape memory alloys, *Proc. SPIE's 5th Annu. Int. Symp. Smart Structures Materials*, Vol. 3324, San Diego, CA, 1998.
20. R. James and M. Wuttig, Magnetostriction of martensite, submitted to *Phil. Mag. A.*, 1997.
21. D. Hall, *Dynamics and vibrations of magnetostrictive transducers*, Ph.D. dissertation, Iowa State Univ., Ames, 1994.
22. F. A. Fischer, *Fundamentals of Electroacoustics*, New York: Interscience, 1955.
23. K. Rolt, History of the flextensional electroacoustic transducer, *J. Acoust. Soc. Amer.*, **87** (3): 1340–1349, 1990.
24. Nat. Defense Res. Committee, *The design and construction of magnetostriction transducers*, Office scientific res. develop., Summary Tech. Rep. Division 6, NDRC, Vol. 13, Washington, DC, 1946.
25. M. Moffett, J. Powers, and A. Clark, Comparison of Terfenol-D and PZT-4 power limitations, *J. Acoust. Soc. Amer.*, **90** (2): 1184–1185, 1991.
26. M. Moffett and W. Clay, Demonstration of the power-handling capability of Terfenol-D, *J. Acoust. Soc. Amer.*, **93** (3): 1653–1654, 1993.
27. T. Akuta, An application of giant magnetostrictive material to high power actuators, in *Workshop on Rare-Earth Magnets and their Applications*, Tokyo: Soc. Non-Traditional Technol., 1989, p. 359.
28. M. Dapino, A. Flatau, and F. Calkins, Statistical analysis of Terfenol-D material properties, *Proc. SPIE Smart Struct. Mater.*, **3041**: 256–267, 1997.
29. M. Dapino et al., Measured Terfenol-D material properties under varied applied magnetic field levels, *Proc. SPIE Smart Struct. Mater.*, **2717**: 697–708, 1996.
30. M. B. Moffett et al., Characterization of Terfenol-D for magnetostrictive transducers, *J. Acoust. Soc. Amer.*, **89**: 1448–1455, 1991.
31. F. Calkins, M. Dapino, and A. Flatau, Effect of prestress on the dynamic performance of a Terfenol-D transducer, *Proc. SPIE Smart Struct. Mater.*, **3041**: 293–304, 1997.
32. J. L. Butler, *Application Manual for the Design of ETREMA Terfenol-D Magnetostrictive Transducers*, Ames, IA: Edge Technol., 1998.
33. M. Rossi, *Acoustics and Electroacoustics*, Norwood, MA: Artech House, 1988.
34. F. T. Calkins and A. B. Flatau, Transducer based measurements of Terfenol-D material properties, *Proc. SPIE Smart Struct. Mater.*, **2717**: 709–719, 1996.
35. A. E. Clark, Magnetostrictive rare earth- $Fe_2$  compounds, in E. P. Wohlfarth (ed.), *Ferromagnetic Materials*, Amsterdam: North-Holland, 1980, Vol. 1, Chap. 7.
36. M. B. Moffett, On the power limitations of sonic transducers, *J. Acoust. Soc. Amer.*, **94** (6): 3503–3505, 1993.
37. R. S. Woolleett, Power limitations of sonic transducers, *IEEE Trans. Sonics Ultrasonics*, **SU-15**: 218–229, 1968.
38. M. B. Moffett and J. M. Powers, Comparison of terfenol-D and PZT-4 power limitations, *J. Acoust. Soc. Amer.*, **90** (2): 1184–85, 1991.
39. F. T. Calkins, *Design, analysis and modeling of giant magnetostrictive transducers*, Ph.D. dissertation, Iowa State Univ., Ames, 1997.
40. F. Claeysen et al., Progress in magnetostrictive sonar transducers, *Conf. Proc. UDT*, Cannes, France, 1993, pp. 246–250.
41. H. C. Hayes, *Sound generating and directing apparatus*, U.S. Patent No. 2,064,911, 1936.
42. W. Toulis, *Flexural-extensional electromechanical transducer*, U.S. Patents No. 3,274,537 and 3,277,433, 1966.
43. L. H. Royster, The flextensional concept: A new approach to the design of underwater acoustic transducers, *Applied Acoustics*, London: Elsevier, 1970, pp. 117–125.
44. G. A. Brigham and L. H. Royster, Present status in the design of flextensional underwater acoustic transducers, *J. Acoust. Soc. Am.*, **46**: 92, 1969.
45. H. C. Merchant, *Underwater transducer apparatus*, U.S. Patent No. 3,258,738, 1966.
46. E. F. Rynne, Innovative approaches for generating high power, low frequency sound, in *Transducers for Sonics and Ultrasonics*, Lancaster, PA: Technomic, 1993, pp. 38–49.
47. F. A. Abbott, *Broadband electroacoustic transducer*, U.S. Patent No. 2,895,062, 1959; reviewed in *J. Acoust. Soc. Amer.* **32**: 310, 1960.
48. C. J. Purcell, Terfenol driver for the barrel-stave projectors, in *Transducers for Sonics and Ultrasonics*, Lancaster, PA: Technomic, 1993, pp. 160–169.

49. D. F. Jones, Flextensional barrel-stave projectors, in *Transducers for Sonics and Ultrasonics*, Lancaster, PA: Technomic, 1993, pp. 150–159.
50. J. A. Pagliarini and R. P. White, A small, wide-band, low frequency, high-power sound source utilizing the flextensional transducer concept, *Oceans 78. The Ocean Challenge*, New York: IEEE, 1978, pp. 333–338.
51. J. C. Debus, J. N. Decarpigny, and B. Hamonic, Analysis of a Class IV flextensional transducer using piece-part equivalent circuit models, in *Transducers for Sonics and Ultrasonics*, Lancaster, PA: Technomic, 1993, pp. 181–1197.
52. F. Claeysen, Giant magnetostrictive alloy actuators, *J. Appl. Electromagn. Mater.*, **5**: 67–73, 1994.
53. G. A. Steel, A 2-kHz magnetostrictive transducer, in *Transducers for Sonics and Ultrasonics*, Lancaster, PA: Technomic, 1993, pp. 250–258.
54. S. C. Butler and J. F. Lindberg, A broadband hybrid magnetostrictive tonpizl transducer, *Proc. UDT*, Sydney, Australia, 1998.
55. S. W. Meeks and R. W. Timme, Rare earth iron magnetostrictive underwater sound transducer, *J. Acoust. Soc. Amer.*, **62**: 1158–1164, 1977.
56. F. Claeysen and D. Boucher, Design of lanthanide magnetostrictive sonar projectors, *Proc. UDT*, Paris, 1991, pp. 1059–1065.
57. H. C. Hayes, U.S. Patent No. 2,005,741, 1935.
58. S. L. Ehrlich and P. D. Frelich, *Directional sonar system*, U.S. Patent No. 3,176,262, 1962.
59. S. L. Ehrlich and P. D. Frelich, *Sonar transducer*, U.S. Patent No. 3,290,646, 1966.
60. S. M. Cohick and J. L. Butler, Rare-earth iron 'square-ring' dipole transducer, *J. Acoust. Soc. Amer.*, **72** (2): 313–315, 1982.
61. J. L. Butler and S. J. Ciosek, Rare earth iron octagonal transducer, *J. Acoust. Soc. Amer.*, **67** (5): 1809–1811, 1990.
62. R. L. Zrostlick, D. H. Hall, and A. B. Flatau, On analog and digital feedback for magnetostrictive transducer linearization, *Proc. SPIE's Smart Structures and Materials*, Vol. 2715, San Diego, CA, 1996, pp. 578–599.
63. M. D. Bryant et al., Active vibration control in structures using magnetostrictive Terfenol-D with feedback and/or neural network controllers, *Proc. Conf. Recent Advances Adaptive Sensory Materials Applications*, Technomic, 1992.
64. J. R. Pratt and A. H. Nayfeh, Smart structures and chatter control, *Proc. 5th Annu. Intern. Symp. Smart Structures Materials*, Vol. 3329, San Diego, 1998, pp. 161–172.
65. H. Nonaka et al., Active vibration control of frame structures with smart structure using magnetostrictive actuators, *Proc. 5th Annu. Int. Symp. Smart Structures Materials*, Vol. 3329, San Diego, 1998, pp. 584–595.
66. L. Jones and E. Garcia, Application of the self-sensing principle to a magnetostrictive structural element for vibration suppression, *ASME Proc. 1994 Int. Mech. Eng. Congr. Expos.*, Chicago, 1994, Vol. 45, pp. 155–165.
67. L. Kiesewetter, Terfenol in linear motors, *Proc. 2nd Inter. Conf. Giant Magnetostrictive Alloys*, 1988.
68. R. C. Roth, The elastic wave motor—a versatile Terfenol driven, linear actuator with high force and great precision, *Proc. 3rd Int. Conf. New Actuators*, AXON Tech., Bremen, German, 1992, pp. 138–141.
69. F. Austin, Smart Terfenol-D powered trailing-edge experiment, *Proc. 5th Annu. Int. Symp. Smart Structures Materials*, Vol. 3326, San Diego, CA, 1998.
70. J. E. Miesner and J. P. Teter, Piezoelectric/magnetostrictive resonant inchworm motor, *Proc. SPIE's Smart Structures Materials*, Vol. 2190, Orlando, FL, 1994, pp. 520–527.
71. B. J. Lund, L. E. Faidley, and A. B. Flatau, Hybrid linear motor design issue analysis, submitted to *SPIE Smart Structures and Integrated Systems Conf.*, Newport Beach, 1999.
72. B. Clephas and H. Janocha, New linear motor with hybrid actuator, *Proc. 4th Annu. Int. Symp. Smart Structures Materials*, Vol. 3041, San Diego, CA, 1997, pp. 316–327.
73. L. Kvarnsjo and G. Engdahl, A new general purpose actuator based on Terfenol-D, *Proc. 3rd Int. Conf. New Actuators*, AXON Tech., Bremen, Germany, 1992, pp. 142–146.
74. T. Akuta, Rotational type actuators with Terfenol-D rods, *Proc. 3rd Int. Conf. New Actuators*, VDI-VDE, Bremen, Germany, 1992, pp. 244–248.
75. J. M. Vranish et al., Magnetostrictive direct drive rotary motor development, *IEEE Trans. Magn.*, **27**: 5355–5357, 1991.
76. F. Claeysen et al., A new resonant magnetostrictive rotating motor, *Proc. 5th Intern. Conf. New Actuators*, AXON Tech., Bremen, Germany, 1996, pp. 272–274.
77. R. Venkataraman, A hybrid actuator, M.S. Thesis, Univ. of Maryland, 1995.
78. J. R. Frederick, *Ultrasonic Engineering*, New York: Wiley, 1965.
79. G. L. Gooberman, *Ultrasonics Theory and Applications*, London: English Univ. Press, 1968.
80. J. Szilard, Ultrasonics, *Encyclopedia of Physical Science and Technology*, Vol. 17, New York: Academic Press, 1992, pp. 153–173.
81. T. T. Hansen, Magnetostrictive materials and ultrasonics, *Chemtech*, 56–69, 1996.
82. A. I. Markov, *Ultrasonic Machining of Intractable Materials*, London: Iliffe Books, 1966.
83. H. E. Bass et al., Ultrasonics, *Encyclopedia of Science and Technology*, 8th ed., New York: McGraw-Hill, 1977.
84. S. Ueha et al., *Ultrasonic Motors Theory and Applications*, Oxford, UK: Clarendon Press, 1993.
85. F. Claeysen et al., Micromotors using magnetostrictive thin films, *Proc. 5th Annu. Int. Symp. Smart Structures Materials*, Vol. 3329, San Diego, CA, 1998.
86. D. M. Dozor, Magnetostrictive wire bonding clamp for semiconductor packaging; initial prototype design, modeling, and experiments, *Proc. 5th Annu. Int. Symp. Smart Structures Materials*, Vol. 3326, San Diego, CA, 1998.
87. O. D. Brimhall and C. J. Hasser, Magnetostrictive linear devices for force reflection in dexterous telemanipulation, *Proc. SPIE's Smart Structures Materials*, Vol. 2190, Orlando, FL, 1994, pp. 508–519.
88. Barry Mersky and Van P. Thompson, *Method and apparatus for imparting low amplitude vibrations to bone and similar hard tissue*, U.S. Patent 5,460,593, 1995.
89. R. P. Cutler, G. E. Sleefe, and R. G. Keefe, Development of a magnetostrictive borehole seismic source, Sandia Report SAN97-0944, Sandia Laboratories, 1977.
90. G. Hartman and J. Sebastian (UDT 1997), *Magnetostrictive system for high-frequency high-cycle fatigue testing*, U.S. Patent No. 5,719,339, 1998.
91. J. B. Restorff, Magnetostrictive materials and devices, *Encyclopedia of Applied Physics*, Vol. 9, VCH, 1994, pp. 229–244.
92. R. P. Culter, G. E. Sleefe, and R. G. Keefe, Development of a magnetostrictive borehole seismic source, Sandia National Labs, Rep. No. SAND97-0944, 1997.
93. W. Fleming, Magnetostrictive torque sensors—Comparison of branch, cross, and solenoidal designs, *Int. Congress and Exposition*, Detroit, 1990, SAE Tech. paper series, 900264, pp. 51–78.
94. W. Fleming, Magnetostrictive torque sensor performance—Nonlinear analysis, *IEEE Trans. Veh. Technol.*, **38**: 159–167, 1989.

95. J. Yamasaki et al., Torque sensors using wire explosion magnetostrictive alloy layers, *IEEE Trans. Magn.*, **MAG-22**: 403–405, 1986.
96. K. Mohri, Review on recent advances in the field of amorphous-metal sensors and transducers, *IEEE Trans. Magn.*, **MAG-20**: 942, 1984.
97. I. Sasada, S. Uramoto, and K. Harada, Noncontact torque sensors using magnetic heads and a magnetostrictive layer on the shaft surface—Application of plasma jet spraying process, *IEEE Trans. Magn.*, **MAG-22**: 406–408, 1986.
98. I. Sasada et al., In-process detection of torque on a drill using magnetostrictive effect, *IEEE Trans. Magn.*, **30**: 4632–4634, 1994.
99. M. Shimada, Magnetostrictive torque sensor and its output characteristics, *J. Appl. Phys.*, **73** (10): 6872–6874, 1993.
100. J. Pratt and A. B. Flatau, Development and analysis of a self-sensing magnetostrictive actuator design, *Proc. SPIE*, **1917**: 952, 1993.
101. J. Pratt, *Design and analysis of a self-sensing Terfenol-D magnetostrictive actuator*, MS. thesis, Iowa State Univ., Ames, 1993.
102. R. C. Fenn and M. J. Gerver, Passive damping and velocity sensing using magnetostrictive transduction, *Proc. SPIE*, **2190**: 216–227, 1994.
103. D. K. Kleinke and H. M. Uras, A noncontact magnetostrictive strain sensor, *Rev. Sci. Instrum.*, **64** (8): 2361–2367, 1993.
104. D. Nyce, Magnetostriction-based linear position sensors, *Sensors*, April, pp. 22–26, 1994.
105. J. Peyrucat, Des distances de 50 metres connués 1 mm pres: C'est l'effect Wiedemann, *Mesures*, **43**: 16, juin 1986.
106. M. Wun-Fogle, H. T. Savage, and M. L. Spano, Enhancement of magnetostrictive effects for sensor applications, *J. Mater. Eng.*, **11** (1): 103–107, 1989.
107. E. Hristoforou and R. E. Reilly, Displacement sensors using soft magnetostrictive alloys, *IEEE Trans. Magn.*, **30**: 2728–2733, 1994.
108. E. Hristoforou and R. E. Reilly, Force sensors based on distortion in delay lines, *IEEE Trans. Magn.*, **28**: 1974–1977, 1992.
109. R. Reilly, Force transducers for use in arrays, U.S. Patent No. 4,924,711, 1990.
110. D. K. Kleinke and H. M. Uras, A magnetostrictive force sensor, *Rev. Sci. Instrum.*, **65** (5): 1699–1710, 1994.
111. J. Seekircher and B. Hoffmann, New magnetoelastic force sensor using amorphous alloys, *Sensors Actuators*, **A21–A23**: 401–405, 1990.
112. K. Mohri and S. Takeuchi, Stress-magnetic effects in iron-rich amorphous alloys and shock-stress sensors with no power, *IEEE Trans. Magn.*, **MAG-17**: 3379–3381, 1981.
113. J. Zakrzewski, Combined magnetoelastic Transducer for Torque and Force measurement, *IEEE Trans. Instrum. Meas.*, **46**: 807–810, 1997.
114. K. A. Bartels, H. Kwun, and J. J. Hanley, Magnetostrictive sensors for the characterization of corrosion in rebars and prestressing strands, *SPIE Proc.*, *Nondestructive Evaluation of Bridges and Highways*, Vol. 2946, Scottsdale, AZ, December 1996.
115. H. Kwun and C. M. Teller, II, *Non destructive evaluation of pipes and tubes using magnetostrictive sensors*, U.S. Patent No. 5,581,037, 1995.
116. J. W. Brophy and C. R. Brett, Guided UT wave inspection of insulated feedwater piping using magnetostrictive sensors, *SPIE Proc.*, **2947**: 205–209, 1996.
117. S. Foner, Review of magnetometry, *IEEE Trans. Magn.*, **MAG-17**: 3358–3363, 1981.
118. R. J. Weber and D. C. Jiles, A Terfenol-D based magnetostrictive diode laser magnetometer, U.S. Dept. Commerce, grant ITA 87-02, 1992.
119. R. Chung, R. Weber, and D. Jiles, A Terfenol-D based magnetostrictive diode laser magnetometer, *IEEE Trans. Magn.*, **27**: 5358–5243, 1991.
120. J. Doherty, S. Arigapudi, and R. Weber, Spectral estimation for a magnetostrictive magnetic field sensor, *IEEE Trans. Magn.*, **30**: 1274–1290, 1994.
121. A. Yariv and H. Windsor, Proposal for detection of magnetic field through magnetostrictive perturbation of optical fibers, *Opt. Lett.*, **5**: 87, 1980.
122. M. Mermelstein, Fundamental limit to the performance of fibre-optic metallic glass DC magnetometers, *Electron. Lett.*, **21**: 1178, 1985.
123. E. Hristoforou, H. Chiriac, and M. Neagu, A new magnetic field sensor based on magnetostrictive delay lines, *IEEE Trans. Instrum. Meas.*, **46**: 632–635, 1997.
124. T. Meydan and M. Elshebani, A magnetostrictive delay line digitizer by using amorphous ribbon materials, *IEEE Trans. Magn.*, **27**: 5250–5252, 1991.
125. T. Worthington et al., A magnetoacoustic keyboard, *IEEE Trans. Magn.*, **MAG-15**: 1797, 1979.
126. K. Shirae and A. Honda, *IEEE Trans. Magn.*, **MAG-17**: 3151, 1981.
127. T. Klinger et al., Magnetostrictive amorphous sensor for biomedical monitoring, *IEEE Trans. Magn.*, **28**: 2400–2402, 1992.
128. T. Klinger et al., 3D-CAD of an amorphous magnetostrictive sensor for monitoring the movements of the human spine, *IEEE Trans. Magn.*, **28**: 2397–2399, 1992.
129. E. Orsier et al., Contactless actuation of giant magnetostriction thin film alloy bimorphs for two-dimensional scanning application, *SPIE Proc.*, **3224**: 98–108, 1997.
130. G. P. Carman and M. Mitrovic, Nonlinear constitutive relations for magnetostrictive materials with applications to 1-D problems, *J. Intell. Materials Syst. Structures*, **6**: 673–684, 1995.
131. S. Kannan and A. Dasgupta, Continuum magnetoelastic properties of Terfenol-D; what is available and what is needed, *Adaptive Materials Symposium*, Summer Meeting of ASME-AMDMD, Univ. of California, Los Angeles, 1995.
132. B. Restorff et al., Preisach modeling of hysteresis in Terfenol-D, *J. Appl. Phys.*, **67**: 5016–5018, 1990.
133. A. A. Adly and I. D. Mayergoyz, Magnetostriction stimulation using anisotropic vector Preisach-type models, *IEEE Trans. Magn.*, **32**: 4773–4775, 1996.
134. R. C. Smith, Modeling techniques for magnetostrictive actuators, *Proc. SPIE Symp. Smart Structures Materials*, Vol. 3041, San Diego, CA, 1997, pp. 243–253.
135. G. Engdahl and A. Berqvist, Loss simulations in magnetostrictive actuators, *J. Appl. Phys.*, **79**: 4689–4691, 1997.
136. V. Basso and G. Bertotti, Hysteresis models for the description of domain wall motion, *IEEE Trans. Magn.*, **32**: 4210–4212, 1996.
137. W. F. Brown, *Magnetoelastic interactions*, Berlin: Springer-Verlag, 1966.
138. R. D. James and D. Kinderlehrer, Theory of magnetostriction with applications to  $TB_xDy_{1-x}Fe_2$ , *Philos. Mag. B*, **68**: 237–274, 1993.
139. E. Della Torea, Fast Preisach based magnetization model and fast inverse hysteresis model, *IEEE Trans. Magn.* submitted.
140. E. C. Stoner and E. P. Wohlfarth, A mechanism of magnetic hysteresis in heterogeneous alloys, *Phil. Trans. Roy. Soc.*, **A240**: 599–642, 1948.

141. E. W. Lee and J. E. Bishop, Magnetic behavior of single-domain particles, *Proc. Phys. Soc.*, **89**: 661, 1966.
142. A. E. Clark, H. T. Savage, and M. L. Spano, Effect of stress on the magnetostriction and magnetization of single crystal  $Tb_{0.27}Dy_{0.73}Fe_2$ , *IEEE Trans. Magn.*, **MAG-20**: 1443–1445, 1984.
143. D. C. Jiles and J. B. Thielke, Theoretical modeling of the effects of anisotropy and stress on the magnetization and magnetostriction of  $Tb_{0.3}Dy_{0.7}Fe_2$ , *J. Magn. Magn. Mater.*, **134**: 143–160, 1994.
144. D. C. Jiles and D. L. Atherton, Theory of ferromagnetic hysteresis, *J. Magn. Magn. Mater.*, **61**: 48, 1986.
145. A. E. Clark et al., Magnetomechanical coupling in Bridgman-grown  $Tb_{0.3}Dy_{0.7}Fe_{1.9}$  at high drive levels, *J. Appl. Phys.* **67**: 5007–5009, 1990.
146. K. Kvarnsjö, On characterization, modeling and application of highly magnetostrictive materials, PhD dissertation, Royal Institute of Technology, TRITA-EEA-9301, Stockholm, Sweden, 1993.
147. C. L. Hom and N. Shankar, A fully coupled constitutive model for electrostrictive ceramic materials, *2nd Int. Conf. Intell. Materials*, ICIM, 1994, pp. 623–624.
148. D. C. Jiles, Frequency dependence of hysteresis curves in conducting magnetic materials, *J. Appl. Phys.*, **76**: 5849–5855, 1994.
149. J. L. Butler and N. L. Lizza, Eddy current loss factor series for magnetostrictive rods, *J. Acoust. Soc. Am.*, **82**: 1997.
150. A. B. Flatau, M. J. Dapino, and F. Calkins, High-bandwidth tunability in a smart passive vibration absorber, *Proc. SPIE Smart Structures Materials*, #3329-19, San Diego, CA, 1998.
151. M. Dapino, R. Smith, and A. Flatau, An active and structural strain model for magnetostrictive transducers, *Proc. SPIE Smart Structures Materials*, #3329-24, San Diego, CA, 1998.

MARCELO J. DAPINO

Iowa State University

FREDERICK T. CALKINS

The Boeing Company

ALISON B. FLATAU

Iowa State University

## MAGNETS FOR MAGNETIC RESONANCE ANALYSIS AND IMAGING

Nuclear magnetic resonance (NMR) was discovered in 1946 by Purcell (1) and Bloch (2). Classically, it is the precession of the spins of nuclei with magnetic moment, subjected to a transverse radio frequency (RF) field in the presence of a longitudinal magnetic field. Nuclear species of biological interest having nonzero magnetic moment are listed in Table 1 together with their Larmor precession frequency-field dependence.

**Table 1. The Larmor Precession Constant for Various Nuclides**

Nuclide	Atomic Number	NMR Frequency (MHz/Tesla)
Hydrogen	1	42.5759
Deuterium	2	6.5357
Carbon	13	10.705
Oxygen	17	5.772
Sodium	23	11.262
Phosphorus	31	17.236

Experimentally, NMR is performed as follows (3,4): nuclei are immersed in a static field  $B_0$ , which results in the development of a net polarization along the field direction, occurring with a time constant  $\tau_1$ . Transitions among their spin states are excited by a high-frequency field  $B_1$ , oriented perpendicular to the static field. In a rotating frame of reference (rotating at the Larmor precession frequency), the magnetization vector of the spin is tilted from a longitudinal direction (along  $B_0$ ) toward the transverse plane. The angle of precession depends on the strength and duration of the applied RF field and is given by

$$\psi = \gamma B_1 \tau_p \quad (1)$$

where  $\tau_p$  is the pulse width and  $\gamma$  is the gyromagnetic ratio.

Following the pulse, the magnetization decays transversely with a time constant  $\tau_2$ , the spin-spin relaxation time. The polarization develops (or decays) along the field with a time constant  $\tau_1$ , the spin-lattice relaxation time.

NMR is the preeminent method for the identification of chemical species in weak solution. It also has useful applications in solid materials. The most exacting specifications for an NMR magnet are imposed by high-resolution NMR. The resonant frequency of a nucleus depends not only on  $B_0$  but also, to a small extent, on the shielding provided by the electronic structure of the chemical compound. This effect is the chemical shift and is distinctive for each chemical species. Thus the resonant frequency of the  $^1H$  nucleus in water is different from that in benzene ( $C_6H_6$ ) or in the methyl or methylene group in alcohol ( $CH_3CH_2OH$ ). These small differences in frequency are typically a few parts per million and provide a means to identify the components of a complex molecule.

Early NMR spectrometers used continuous wave (CW) methods in which the frequency of the  $B_1$  field would be changed slowly and the absorption of a tank circuit enclosing the sample would be recorded as a spectrum of power absorption versus frequency. At the resonant frequency a sharp increase in absorption would be observed. The width of the peak depended, among other things, on the magnification  $Q$  of the tank circuit.

In modern NMR, a pulse of RF of sufficient strength and duration is applied to the sample so that all the spins are excited. The pulse is then switched off, and the signals emitted at various frequencies by the sample during relaxation of the spins are monitored. A Fourier analysis of the signal then transforms the time-dependent spectrum into a frequency-dependent signal, thus revealing the resonance peaks associated with the chemical shifts (3,4).

The uniformity of the static field  $B_0$  is the key to high-resolution NMR and to sharp images in magnetic resonance imaging (MRI). A uniform field allows large numbers of nuclei to precess at exactly the same frequency, thus generating a strong signal of narrow bandwidth. The underlying theory and practice of high-homogeneity superconducting magnets is described in this section. MRI magnets differ from those used for NMR analysis in that spatial distribution of either signal strength or  $\tau_1$  or  $\tau_2$  relaxation times are measured over a volume far greater than that of a sample for chemical analysis. In MRI, the predominant nuclear species examined is hydrogen in water. Density or  $\tau_1$  or  $\tau_2$  is measured on planes

Copyright of Encyclopedia of Electrical & Electronics Engineering is the property of John Wiley & Sons, Inc. / Engineering and its content may not be copied or emailed to multiple sites or posted to a listserv without the copyright holder's express written permission. However, users may print, download, or email articles for individual use.

Copyright of Encyclopedia of Electrical & Electronics Engineering is the property of John Wiley & Sons, Inc. / Engineering and its content may not be copied or emailed to multiple sites or posted to a listserv without the copyright holder's express written permission. However, users may print, download, or email articles for individual use.